DC-derived IL-15 controls endotoxin shock induction by controlling the production of IL-12, IFN-γ, and TNF-α, as DC-depleted mice produced these cytokines at much reduced levels, and WT DC-injected IL-15$^{-/-}$ mice became sensitive to endotoxin shock. Contrary to IL-15$^{-/-}$ mice, *P. acnes*–primed IL-18$^{-/-}$ mice showed much higher TNF-α production and susceptibility to LPS-induced endotoxin shock (58). Together with our results, IL-15 and IL-18 function apparently through distinct pathways in terms of TNF-α production, and IL-15 induces, whereas IL-18 suppresses, TNF-α production.

Collectively, we propose here that DC-derived IL-15 is a master regulator of inflammatory responses in granulomatous liver diseases and related endotoxin shock. Indeed, DC-derived IL-15 regulates the production of IL-12p70, IFN-γ, TNF-α, and downstream CCL2/3/4. Given that elevated IL-15 production and IL-15–expressing cells are evident in RA (13, 14), inflammatory bowel disease (17), type C chronic liver disease (18), sarcoidosis (19), multiple sclerosis (20), and celiac disease (59), it is important to further investigate the roles of IL-15 in these inflammatory diseases and search for the propriety of IL-15 as a target for the development of antiinflammatory drugs.

MATERIALS AND METHODS

Mice. B6–IL-15$^{-/-}$ (IL-15$^{-/-}$) mice (6) were purchased from Taconic, and B6-RAG2$^{-/-}$ (RAG2$^{-/-}$) mice were provided by Taconic and Central Laboratories for Experimental Animals. B6–IFN-γ$^{-/-}$ mice were purchased from The Jackson Laboratory. To obtain B6–IL-15$^{-/-}$RAG2$^{-/-}$ mice (IL-15$^{-/-}$ × RAG2$^{-/-}$), F_1 mice were backcrossed with RAG2$^{-/-}$ mice, and the obtained IL-15$^{+/-}$RAG2$^{-/-}$ mice were intercrossed. The offspring were genotyped for IL-15, and IL-15$^{-/-}$RAG2$^{-/-}$ mice were used for experiments. B6-CD11c-DTR-GFP mice (41) were provided by Steffen Jung, Dan R. Littman, and Richard A. Lang (New York University School of Medicine, New York, NY). All mice were maintained in our specific pathogen-free animal facility, and experiments were performed between 6–12 wk of age in accordance with the guidelines of the Institutional Animal Care Committee of Akita University and Keio University School of Medicine.

Histologic and immunohistochemical analysis. Frozen livers embedded in OCT compound (Sakura Finetek) were sliced into 5-μm-thick sections and fixed with 1% paraformaldehyde and stained with Mayer's hematoxylin and eosin (H&E). Sections of livers were observed with a microscope (DM4500 B; Leica). For CD11c immunostaining, acetone-fixed 5-μm fresh-frozen tissue sections were incubated with biotinylated anti-CD11c mAb (clone, N418; eBioscience) overnight at 4°C and with streptavidin-conjugated horseradish peroxidase (HRP; PerkinElmer). Sections were immunostained using 3,3′-diaminobenzidine (DAB) substrate liquid (DakoCytomation). Slides were counterstained with Mayer's hematoxylin. For CD11c and IL-15 double immunofluorescence staining, acetone-fixed 5-μm fresh-frozen tissue sections were incubated with FITC-conjugated anti-CD11c (clone, N418; eBioscience) and biotinylated goat anti-mouse IL-15 polyclonal antibody (R&D Systems) for 1 h at room temperature. Sections were further stained with streptavidin-conjugated PE (eBioscience) for 30 min at room temperature and observed by fluorescence microscopy.

Measurement of serum chemokines, cytokines, GPT, and GOT. Levels of IL-12p70, IFN-γ, TNF-α, and CCL2/3/4 in the sera were measured by ELISA kits (IL-12p70, IFN-γ, and TNF-α were obtained from BD Biosciences; CCL2/3/4 was obtained from R&D Systems), according to the manufacturer's instructions. The concentrations of cytokines were determined using a data analysis program (Softmax PRO; Molecular Devices). Serum GPT and GOT levels were determined with Fuji Dri-Chem 5500V (Fuji Medical System), according to the manufacturer's instructions.

Generation of anti–mouse IL-15 mAb and ELISA for mouse IL-15. To detect mouse IL-15 protein, mAbs specific for mouse IL-15 were generated by immunizing mouse IL-15 into Lewis rat. Using conventional methods, spleen cells isolated from the immunized rat were fused with X63-Ag8.653 myeloma cells, and limiting dilution for hybridoma cells was performed. Positive clones producing anti–IL-15 mAb were screened based on the binding capacity to coated mouse IL-15. Among the mAbs, AIO2 and AIO3 clones were further selected as neutralizing mAbs based on the inhibition of IL-15–dependent CTLL-2 cell proliferation. In brief, 5 × 10^4 CTLL-2 cells were cultured with 10 ng/ml IL-15 or IL-2 in the presence or absence of 10 μg/ml AIO2 and AIO3 for 24 h and pulsed with [^{3}H]thymidine for an additional 8 h. For mouse IL-15 sandwich ELISA, microwells were coated with AIO3 overnight at 4°C and incubated with Block Ace (Dainippon Pharmaceutical) for 90 min. The diluted serum samples were incubated for 2 h, then for 60 min with biotinylated goat anti–mouse IL-15 antibody (R&D Systems) and for 60 min with avidin-HRP (Sigma-Aldrich). The absorbance of substance released from the substrate was measured at 450 nm. The IL-15 concentrations in samples were determined using Softmax PRO, based on a standard curve of recombinant mouse IL-15.

Reagents and in vivo treatment. Mice were injected with either 0.5 mg of heat-killed *P. acnes* (American Type Culture Collection) or 1 mg of zymosan (Sigma-Aldrich). 6 d later, the amounts of LPS indicated in the figures (*Escherichia coli* O55:B5; Sigma-Aldrich) were further injected into *P. acnes*– and zymosan-primed mice, respectively, to induce endotoxin shock. To deplete NK cells, 300 μg/200 μl of polyclonal anti-asialo GM1 (Wako) was injected. To neutralize IL-15 in vivo, 0.5 mg AIO2 was injected. For systemic DC depletion in vivo, CD11c-DTR-GFP mice were injected intraperitoneally with 100 ng/body of diphtheria toxin (Sigma-Aldrich).

DC preparation, detection of apoptosis, and adoptive transfer. DCs were prepared from spleens as previously described (8). In brief, collagenase-digested spleen cells were suspended in a 28% BSA solution in 1.08 g/ml PBS, overlaid with 1 ml FCS-free RPMI 1640 medium (Sigma-Aldrich), and centrifuged at 9,500 *g* for 20 min at 4°C. The cells at the interface were collected, washed, and resuspended. DCs were further purified using anti-CD11c (clone N418) microbeads with an autoMACS separation system (Miltenyi Biotec). To detect apoptotic DCs, 5 × 10^5 DCs were cultured in vitro for 6 h and incubated for 15 min at room temperature in 500 μl annexin V binding buffer with 150 ng/ml annexin V (R&D Systems) or for 10 min at 4°C in 500 μl PBS with 2 μg/ml propidium idodide (Sigma-Aldrich), respectively. For generation of BMDCs, WT and IL-15$^{-/-}$ BM cells were cultured at 1.5 × 10^6 cells/ml in 10% FCS RPMI 1640 medium in the presence of 10 ng/ml GM-CSF (RDI Division of Fitzgerald Industries). After 3 d of culture, half of the medium was exchanged with a fresh one. After 6 d of culture, BMDCs were purified using anti-CD11c microbeads with an autoMACS separation system. For adoptive transfer experiments, 1 × 10^6 BMDCs were intravenously injected into IL-15$^{-/-}$ mice.

Qualitative determination of intracellular GSH with ACAS. The procedures have previously been described (44). In brief, 300 μl of a suspension of splenic DCs, adjusted to a density of 3 × 10^5 cells/ml in an RPMI 1640 (phenol red free) medium, were applied into a chamber slide (Lab-Tek; Nunc) and incubated for 3 h. After washing, 300 μl of 10 μM monochlorobiman was added, and the reaction was conducted for 30 min. The fluorescence intensity was monitored by argon-ion laser cytometry with a workstation (ACAS 570; Meridian Instruments). Intracellular GSH levels were detected with an excitation wavelength of 350 nm and an emission wavelength of 460 nm.

Online supplemental material. Fig. S1 shows granuloma formation in the liver of NK cell–depleted RAG-2$^{-/-}$ mice. Fig. S2 shows the level of

serum CCL2 in NK cell–depleted RAG-2$^{-/-}$ mice. Fig. S3 shows reductive status in *P. acnes*–stimulated IL-15$^{-/-}$ DCs.

We thank M. Shibata, N. Kakizaki, and M. Motouchi for animal care; M. Kondo and K. Maekawa for screening of hybridoma cells and mAb purification; K. Yamashita and Y. Abe for experimental support; and T. Yoshimoto and K. Nakanishi for Kupffer cell isolation and critical reading of the manuscript.

This work was supported in part by the Toray Science Foundation (T.Ohteki); the Uehara Memorial Foundation (T.Ohteki); the Takeda Science Foundation (T. Ohteki); the Novartis Foundation for the Promotion of Science (T. Ohteki); the Sankyo Foundation for Life Science (T. Ohteki); grants-in-aid for Scientific Research on Priority Areas from the Ministry of Education, Culture, Sports, Science and Technology of Japan (14021110 to S. Koyasu; 16017212 and 16043204 to T. Ohteki); the 21st Century Center of Excellence Program; a Keio University special grant-in-aid for Innovative Collaborative Research Projects; and the Uehara Memorial Foundation special project research grant (to S. Koyasu). H. Tada is supported by a research fellowship from the Japan Society for the Promotion of Science for Young Scientists.

The authors have no conflicting financial interests.

Submitted: 19 June 2006
Accepted: 14 August 2006

REFERENCES

1. Ohteki, T., S. Ho, H. Suzuki, T.W. Mak, and P.S. Ohashi. 1997. Role for IL-15/IL-15 receptor β-chain in natural killer 1.1$^+$ T cell receptor-αβ$^+$ cell development. *J. Immunol.* 159:5931–5935.
2. Ogasawara, K., S. Hida, N. Azimi, Y. Tagaya, T. Sato, T. Yokochi-Fukada, T.A. Waldmann, T. Taniguchi, and S. Taki. 1998. Requirement for IRF-1 in the microenvironment supporting development of natural killer cells. *Nature.* 391:700–703.
3. Ohteki, T., H. Yoshida, T. Matsuyama, G.S. Duncan, T.W. Mak, and P.S. Ohashi. 1998. The transcription factor interferon regulatory factor 1 (IRF-1) is important during the maturation of natural killer 1.1$^+$ T cell receptor-α/β$^+$ (NK1$^+$ T) cells, natural killer cells, and intestinal intraepithelial T cells. *J. Exp. Med.* 187:967–972.
4. Lodolce, J.P., D.L. Boone, S. Chai, R.E. Swain, T. Dassopoulos, S. Trettin, and A. Ma. 1998. IL-15 receptor maintains lymphoid homeostasis by supporting lymphocyte homing and proliferation. *Immunity.* 9:669–676.
5. Waldmann, T.A., and Y. Tagaya. 1999. The multifaceted regulation of interleukin-15 expression and the role of this cytokine in NK cell differentiation and host response to intracellular pathogens. *Annu. Rev. Immunol.* 17:19–49.
6. Kennedy, M.K., M. Glaccum, S.N. Brown, E.A. Butz, J.L. Viney, M. Embers, N. Matsuki, K. Charrier, L. Sedger, C.R. Willis, et al. 2000. Reversible defects in natural killer and memory CD8 T cell lineages in interleukin 15–deficient mice. *J. Exp. Med.* 191:771–780.
7. Mattei, F., G. Schiavoni, F. Belardelli, and D.F. Tough. 2001. IL-15 is expressed by dendritic cells in response to type I IFN, double-stranded RNA, or lipopolysaccharide and promotes dendritic cell activation. *J. Immunol.* 167:1179–1187.
8. Ohteki, T., K. Suzue, C. Maki, T. Ota, and S. Koyasu. 2001. Critical role of IL-15–IL-15R for antigen-presenting cell functions in the innate immune response. *Nat. Immunol.* 2:1138–1143.
9. Kuwajima, S., T. Sato, K. Ishida, H. Tada, H. Tezuka, and T. Ohteki. 2006. Interleukin 15–dependent crosstalk between conventional and plasmacytoid dendritic cells is essential for CpG-induced immune activation. *Nat. Immunol.* 7:740–746.
10. Becker, T.C., E.J. Wherry, D. Boone, K. Murali-Krishna, R. Antia, A. Ma, and R. Ahmed. 2002. Interleukin 15 is required for proliferative renewal of virus-specific memory CD8 T cells. *J. Exp. Med.* 195:1541–1548.
11. Goldrath, A.W., P.V. Sivalumar, M. Glaccum, M.K. Kennedy, M.J. Bevan, C. Benoist, D. Mathis, and E.A. Butz. 2002. Cytokine requirements for acute and basal homeostatic proliferation of naive and memory CD8$^+$ T cells. *J. Exp. Med.* 195:1515–1522.
12. Schluns, K.S., K. Williams, A. Ma, X.X. Zheng, and L. Lefrançois. 2002. Requirement for IL-15 in the generation of primary and memory antigen-specific CD8 T cells. *J. Immunol.* 168:4827–4831.
13. McInnes, I.B., J. Al-Mughales, M. Field, B.P. Leung, F.-P. Huang, R. Dixon, R.D. Sturrock, P.C. Wilkinson, and F.Y. Liew. 1996. The role of interleukin 15 in T-cell migration and activation in rheumatoid arthritis. *Nat. Med.* 2:175–182.
14. McInnes, I.B., B.P. Leung, R.D. Sturrock, M. Field, and F.Y. Liew. 1997. Interleukin-15 mediates T cell-dependent regulation of tumor necrosis factor-α production in rheumatoid arthritis. *Nat. Med.* 3:189–195.
15. Ruchatz, H., B.P. Leung, X. Wei, I.B. McInnes, and F.Y. Liew. 1998. Soluble IL-15 receptor α-chain administration prevents murine collagen-induced arthritis: a role for IL-15 in development of antigen-induced immunopathology. *J. Immunol.* 160:5654–5660.
16. Ferrari-Lacraz, S., E. Zanelli, M. Neuberg, E. Donskoy, Y.S. Kim, X.X. Zheng, W.W. Hancock, W. Maslinski, X.C. Li, T.B. Strom, and T. Moll. 2004. Targeting IL-15 receptor-bearing cells with an antagonist mutant IL-15/Fc protein prevents disease development and progression in murine collagen-induced arthritis. *J. Immunol.* 173:5818–5826.
17. Kirman, I., and O.H. Nielsen. 1996. Increased numbers of interleukin-15-expressing cells in active ulcerative colitis. *Am. J. Gastroenterol.* 91: 1789–1794.
18. Kakumu, S., A. Okumura, T. Ishikawa, M. Yano, A. Enomoto, H. Nishimura, K. Yoshioka, and Y. Yoshikai. 1997. Serum levels of IL-10, IL-15 and soluble tumour necrosis factor-alpha (TNF-α) receptors in type C chronic liver disease. *Clin. Exp. Immunol.* 109:458–463.
19. Agostini, C., L. Trentin, M. Facco, R. Sancetta, A. Cerutti, C. Tassinari, L. Cimarosto, F. Adami, A. Cipriani, R. Zambello, and G. Semenzato. 1996. Role of IL-15, IL-2 and their receptors in the development of T cell alveolitis in pulmonary sarcoidosis. *J. Immunol.* 157:910–918.
20. Kivisäkk, P., D. Matusevicius, B. He, M. Söderström, S. Fredrikson, and H. Link. 1998. IL-15 mRNA expression is up-regulated in blood and cerebrospinal fluid mononuclear cells in multiple sclerosis (MS). *Clin. Exp. Immunol.* 111:193–197.
21. Senaldi, G., S. Yin, C.L. Shaklee, P.-F. Piguet, T.W. Mak, and T.R. Ulich. 1996. *Corynebacterium parvum*- and *Mycobacterium bovis* bacillus Calmette-Guérin-induced granuloma formation is inhibited in TNF receptor I (TNF-RI) knockout mice and by treatment with soluble TNF-RI. *J. Immunol.* 157:5022–5026.
22. Marino, M.W., A. Dunn, D. Grail, M. Inglese, Y. Noguchi, E. Richards, A. Jungbluth, H. Wada, M. Moore, B. Williamson, et al. 1997. Characterization of tumor necrosis factor-deficient mice. *Proc. Natl. Acad. Sci. USA.* 94:8093–8098.
23. Tsuji, H., N. Mukaida, A. Harada, S. Kaneko, E. Matsushita, Y. Nakamura, H. Tsutsui, H. Okamura, K. Nakanishi, Y. Tagawa, et al. 1999. Alleviation of lipopolysaccharide-induced acute liver injury in *Propionibacterium acnes*-primed IFN-γ-deficient mice by a concomitant reduction of TNF-α, IL-12, and IL-18 production. *J. Immunol.* 162: 1049–1055.
24. Yoneyama, H., K. Matsuno, Y. Zhang, M. Murai, M. Itakura, S. Ishikawa, G. Hasegawa, M. Naito, H. Asakura, and K. Matsushima. 2001. Regulation by chemokines of circulating dendritic cell precursors and the formation of portal tract–associated lymphoid tissue in a granulomatous liver disease. *J. Exp. Med.* 193:35–49.
25. Sanguedolce, M.V., C. Capo, P. Bongrand, and J.-L. Mege. 1992. Zymosan-stimulated tumor necrosis factor-α production by human monocytes: down-modulation by phorbol ester. *J. Immunol.* 148:2229–2236.
26. Underhill, D.M., A. Ozinsky, A. Hajjar, A. Stevens, C.B. Wilson, M. Bassetti, and A. Aderem. 1999. The Toll-like receptor 2 is recruited to macrophage phagosomes and discriminates between pathogens. *Nature.* 401:811–815.
27. Young, S.-H., J. Ye, D.G. Frazer, X. Shi, and V. Castranova. 2001. Molecular mechanism of tumor necrosis-α production in 1,3-β-glucan (zymosan)-activated macrophages. *J. Biol. Chem.* 276:20781–20787.
28. Daum, T., and M.S. Rohrbach. 1992. Zymosan induces selective release of arachidonic acid from rabbit alveolar macrophages via stimulation of a β-glucan receptor. *FEBS Lett.* 309:119–122.
29. Nobel, P.W., P.M. Henson, C. Lucas, M. Mora-Worms, P.C. Carré, and D.W.H. Riches. 1993. Transforming growth factor-β primes macrophages to express inflammatory gene products in response to particulate stimuli by an autocrine/paracrine mechanism. *J. Immunol.* 151:979–989.

30. Okazaki, M., N. Chiba, Y. Adachi, N. Ohno, and T. Yadomae. 1996. Signal transduction pathway on β-glucans-triggered hydrogen peroxide production by murine peritoneal macrophages in vitro. *Biol. Pharm. Bull.* 19:18–23.
31. Jinnouchi, K., Y. Terasaki, S. Fujiyama, K. Tomita, W.A. Kuziel, N. Maeda, K. Takahashi, and M. Takeya. 2003. Impaired hepatic granuloma formation in mice deficient in C-C chemokine receptor 2. *J. Pathol.* 200:406–416.
32. Yoshimoto, T., K. Nakanishi, S. Hirose, K. Hiroishi, H. Okamura, Y. Takemoto, A. Kanamaru, T. Hada, T. Tamura, E. Kakishita, and K. Higashino. 1992. High serum IL-6 level reflects susceptible status of the host to endotoxin and IL-1/tumor necrosis factor. *J. Immunol.* 148:3596–3603.
33. Gu, Y., K. Kuida, H. Tsutsui, G. Ku, K. Hsiao, M.A. Fleming, N. Hayashi, K. Higashino, H. Okamura, K. Nakanishi, et al. 1997. Activation of interferon-γ inducing factor mediated by interleukin-1β converting enzyme. *Science.* 275:206–209.
34. Merlin, T., A. Sing, P.J. Nielsen, C. Galanos, and M.A. Freudenberg. 2001. Inherited IL-12 unresponsiveness contributes to the high LPS resistance of the LPS (d) C57BL/10ScCr mouse. *J. Immunol.* 166:566–573.
35. Sun, X.M., W. Hsueh, and G. Torre-Amione. 1990. Effects of in vivo "priming" on endotoxin-induced hypotension and tissue injury. The role of PAF and tumor necrosis factor. *Am. J. Pathol.* 136:949–956.
36. Pfeffer, K., T. Matsuyama, T.M. Kündig, A. Wakeham, K. Wiegmann, P.S. Ohashi, M. Krönke, and T.W. Mak. 1993. Mice deficient for the 55 kd tumor necrosis factor receptor are resistant to endotoxic shock, yet succumb to *L. monocytogenes* infection. *Cell.* 73:457–467.
37. Rothe, J., W. Lesslauer, H. Lotscher, Y. Lang, P. Koebel, F. Kontgen, A. Althage, R. Zinkernagel, M. Steinmetz, and H. Bluethmann. 1993. Mice lacking the tumour necrosis factor receptor 1 are resistant to TNF-mediated toxicity but highly susceptible to infection by *Listeria monocytogenes. Nature.* 364:798–802.
38. Car, B.D., V.M. Eng, B. Schnyder, L. Ozmen, S. Huang, P. Galley, D. Heumann, M. Aguet, and B. Ryffel. 1994. Interferon γ receptor–deficient mice are resistant to endotoxic shock. *J. Exp. Med.* 179: 1437–1444.
39. Pasparakis, M., L. Alexopoulou, V. Episkopou, and G. Kollias. 1996. Immune and inflammatory responses in TNFα-deficient mice:a critical requirement for TNFα in the formation of primary B cell follicles, follicular dendritic cell networks and germinal centers, and in the maturation of the humoral immune response. *J. Exp. Med.* 184:1397–1411.
40. Dubois, S.P., T.A. Waldmann, and J.R. Muller. 2005. Survival adjustment of mature dendritic cells by IL-15. *Proc. Natl. Acad. Sci. USA.* 102:8662–8667.
41. Jung, S., D. Unutmaz, P. Wong, G. Sano, K. De los Santos, T. Sparwasser, S. Wu, S. Vuthoori, K. Ko, F. Zavala, et al. 2002. In vivo depletion of CD11c$^+$ dendritic cells abrogates priming of CD8$^+$ T cells by exogenous cell-associated antigens. *Immunity.* 17:211–220.
42. Peterson, J.D., L.A. Herzenberg, K. Vasquez, and C. Waltenbaugh. 1998. Glutathione levels in antigen-presenting cells modulate Th1 versus Th2 response patterns. *Proc. Natl. Acad. Sci. USA.* 95:3071–3076.
43. Murata, Y., M. Amao, J. Yoneda, and J. Hamuro. 2002. Intracellular thiol redox status of macrophages directs the Th1 skewing in thioredoxin transgenic mice during aging. *Mol. Immunol.* 38:747–757.
44. Murata, Y., T. Ohteki, S. Koyasu, and J. Hamuro. 2002. IFN-γ and pro-inflammatory cytokine production by antigen-presenting cells is dictated by intracellular thiol redox status regulated by oxygen tension. *Eur. J. Immunol.* 32:2866–2873.
45. Murata, Y., T. Shimamura, and J. Hamuro. 2002. The polarization of T(h)1/T(h)2 balance is dependent on the intracellular thiol redox status of macrophages due to the distinctive cytokine production. *Int. Immunol.* 14:201–212.
46. Ma, A., R. Koka, and P. Burkett. 2006. Diverse functions of IL-2, IL-5, and IL-7 in lymphoid homeostasis. *Annu. Rev. Immunol.* 24:657–679.
47. Rückert, R., K. Brandt, E. Bulanova, F. Mirghomizadeh, R. Paus, and S. Bulfone-Paus. 2003. Dendritic cell-derived IL-15 controls the induction of CD8 T cell immune responses. *Eur. J. Immunol.* 33:3493–3503.
48. Lodolce, J.P., P.R. Burkett, D.L. Boone, M. Chien, and A. Ma. 2001. T cell–independent interleukin-15α signals are required for bystander proliferation. *J. Exp. Med.* 194:1187–1194.
49. Judge, A.D., X. Zhang, H. Fujii, C.D. Surh, and J. Sprent. 2002. Interleukin-15 controls both proliferation and survival of a subset of memory-phenotype CD8$^+$ T cells. *J. Exp. Med.* 196:935–946.
50. Burkett, P.R., R. Koka, M. Chien, S. Chai, F. Chan, A. Ma, and D.L. Boone. 2003. IL-15Rα expression on CD8$^+$ T cells is dispensable for T cell memory. *Proc. Natl. Acad. Sci. USA.* 100:4724–4729.
51. Burkett, P.R., R. Koka, M. Chien, S. Chai, D.L. Boone, and A. Ma. 2004. Coordinate expression and trans presentation of interleukin (IL)-15Rα and IL-15 supports natural killer cell and memory CD8$^+$ T cell homeostasis. *J. Exp. Med.* 200:825–834.
52. Schluns, K.S., K.D. Klonowski, and L. Lefrancois. 2004. Transregulation of memory CD8 T-cell proliferation by IL-15Rα$^+$ bone marrow-derived cells. *Blood.* 103:988–994.
53. Schluns, K.S., E.C. Nowak, A. Cabrera-Hernandez, L. Puddington, L. Lefrancois, and H.L. Aguila. 2004. Distinct cell types control lymphoid subset development by means of IL-15 and IL-15 receptor α expression. *Proc. Natl. Acad. Sci. USA.* 101:5616–5621.
54. Kuziel, W.A., S.J. Morgan, T.C. Dawson, S. Griffin, O. Smithies, K. Ley, and N. Maeda. 1997. Severe reduction in leukocyte adhesion and monocyte extravasation in mice deficient in CC chemokine receptor 2. *Proc. Natl. Acad. Sci. USA.* 94:12053–12058.
55. Ichiyasu, H., M. Suga, A. Matsukawa, K. Iyonaga, T. Mizobe, T. Takahashi, and M. Ando. 1999. Functional roles of MCP-1 in *Propionibacterium acnes*-induced, T cell-mediated pulmonary granulomatosis in rabbits. *J. Leukoc. Biol.* 65:482–491.
56. Peters, W., H.M. Scott, H.F. Chambers, J.L. Flynn, I.F. Charo, and J.D. Ernst. 2001. Chemokine receptor 2 serves an early and essential role in resistance to *Mycobacterium tuberculosis. Proc. Natl. Acad. Sci. USA.* 98:7958–7963.
57. Kamijo, R., J. Le, D. Shapiro, E.A. Havell, S. Huang, M. Aguet, M. Bosland, and J. Vilcek. 1993. Mice that lack the interferon-γ receptor have profoundly altered responses to infection with Bacillus Calmette-Guerin and subsequent challenge with lipopolysaccharide. *J. Exp. Med.* 178:1435–1440.
58. Sakao, Y., K. Takeda, H. Tsutsui, T. Kaisho, F. Nomura, H. Okamura, K. Nakanishi, and S. Akira. 1999. IL-18-deficient mice are resistant to endotoxin-induced liver injury but highly susceptible to endotoxin shock. *Int. Immunol.* 11:471–480.
59. Hüe, S., J.-J. Mention, R.C. Monteiro, S. Zhang, C. Cellier, J. Schmitz, V. Verkarre, N. Fodil, S. Bahram, N. Cerf-Bensussan, and S.C. Caillat-Zucman. 2004. A direct role for NKG2D/MICA interaction in villous atrophy during celiac disease. *Immunity.* 21:367–377.

Synergistic Pathogenic Effects of Combined Mouse Monoclonal Anti-Desmoglein 3 IgG Antibodies on Pemphigus Vulgaris Blister Formation

Hiroshi Kawasaki[1], Kazuyuki Tsunoda[1,2], Tsuyoshi Hata[1,3], Ken Ishii[1], Taketo Yamada[4] and Masayuki Amagai[1]

Pemphigus vulgaris (PV) is an autoimmune blistering disease caused by anti-desmoglein 3 (Dsg3) IgG antibodies. Previously, we generated an active mouse model for PV by adoptive transfer of splenocytes from immunized or naive $Dsg3^{-/-}$ mice. In this study, we isolated 10 anti-Dsg3 IgG mAbs (NAK-series) from PV model mice generated by transfer of naive $Dsg3^{-/-}$ splenocytes. We characterized their epitopes using domain-swapped and point-mutated Dsg1/Dsg3 molecules and examined their pathogenic activities in blister formation in three different assays. In a passive transfer model using neonatal mice, eight of 10 NAK mAbs showed pathogenic activity when injected together with half the minimum pathogenic dose of anti-Dsg1 IgG autoantibodies from pemphigus foliaceus (PF) patients. None of the mAbs could induce the PV phenotype when individual hybridoma clones were inoculated by peritoneal injection into adult $Rag2^{-/-}$ mice. NAK mAbs displayed a range of potency in an *in vitro* dissociation assay using primary cultured mouse keratinocytes. Interestingly, when multiple hybridoma clones recognizing different epitopes were inoculated in combination, recipient mice developed the PV phenotype. *In vitro* dissociation assays confirmed that combined NAK mAbs had synergistic pathogenic effects. These findings indicate that although an individual anti-Dsg3 IgG is not sufficient to cause blistering in adult mice, several together can induce the PV phenotype. These mAbs will provide a valuable tool to investigate the molecular mechanisms of blister formation, mimicking the effects of the polyclonal IgG antibodies found in patients.

Journal of Investigative Dermatology (2006) **126,** 2621–2630. doi:10.1038/sj.jid.5700450; published online 13 July 2006

INTRODUCTION

Pemphigus vulgaris (PV) is a fatal autoimmune blistering disease of the skin and mucous membranes (Amagai, 2003), which is characterized clinically by flaccid blisters and erosions, and histopathologically by the loss of cell–cell adhesion between basal and suprabasal keratinocytes, resulting in suprabasal acantholysis. The target antigen of PV is desmoglein 3 (Dsg3), a desmosomal transmembrane glycoprotein that belongs to the cadherin gene superfamily of Ca^{2+}-dependent cell–cell adhesion molecules (Amagai *et al.*, 1991; Amagai, 1996). Compelling evidence indicates that IgG autoantibodies against Dsg3 in PV play a primary pathogenic role in blister formation (Anhalt *et al.*, 1982; Amagai *et al.*, 1992, 1998; Mahoney *et al.*, 1999).

Previously, we developed a mouse model for PV using $Dsg3^{-/-}$ mice, which should not acquire immunological tolerance to Dsg3 (Amagai *et al.*, 2000b). After immunization of $Dsg3^{-/-}$ mice with recombinant extracellular domains of mouse Dsg3, we adoptively transferred splenocytes from the immunized mice into $Rag2^{-/-}$ recipient mice that express Dsg3. The transferred $Dsg3^{-/-}$ lymphocytes stably produced anti-Dsg3 IgG and the recipient mice developed a PV phenotype, including oral erosions with histological suprabasilar acantholysis and telogen hair loss (Koch *et al.*, 1997). Subsequently, we demonstrated that the adoptive transfer of naive splenocytes from nonimmunized $Dsg3^{-/-}$ mice to $Rag2^{-/-}$ recipients also induced the production of anti-Dsg3 IgG and the PV phenotype (Aoki-Ota *et al.*, 2004). Antibody production and the appearance of the PV phenotype were delayed by approximately 2 weeks in mice receiving naive splenocytes compared to those receiving immunized splenocytes. However, once the PV phenotype developed, there were no apparent differences in disease severity between mice induced by the two methods. Interestingly, the anti-Dsg3 IgG titers were markedly lower in mice that received naive splenocytes than in mice that received immunized

[1]*Department of Dermatology, Keio University School of Medicine, Shinjuku-ku, Tokyo, Japan;* [2]*Department of Dentistry and Oral Surgery, Keio University School of Medicine, Shinjuku-ku, Tokyo, Japan;* [3]*R&D Division, KOSÉ Corporation, Tokyo, Japan and* [4]*Department of Pathology, Keio University School of Medicine, Shinjuku-ku, Tokyo, Japan*

Correspondence: Dr Masayuki Amagai, Department of Dermatology, Keio University School of Medicine, 35 Shinanomachi, Shinjuku-ku, Tokyo 160-8582, Japan. E-mail: amagai@sc.itc.keio.ac.jp

Abbreviations: Dsg, desmoglein; hDsg, human desmoglein; mDsg, mouse desmoglein; PF, pemphigus foliaceus; PV, pemphigus vulgaris

Received 17 December 2005; revised 19 March 2006; accepted 8 April 2006; published online 13 July 2006

splenocytes, suggesting that the antibodies generated in the former are more potent than those in the latter. Conformational epitope mapping in model mice revealed that anti-Dsg3 IgG were predominantly raised against the middle to C-terminal extracellular domains of mouse Dsg3, where amino-acid residues are less conserved among desmoglein isoforms. PV model mice receiving naive splenocytes produced antibodies against the N-terminal domain of Dsg3 more frequently than mice receiving immunized splenocytes (Anzai *et al.*, 2004).

We isolated eight anti-Dsg3 IgG mAbs from PV model mice that received immunized Dsg3$^{-/-}$ splenocytes (the AK series) (Tsunoda *et al.*, 2003). Two of these mAbs were capable of inducing the loss of cell-cell adhesion in keratinocytes, as determined in a passive transfer model using neonatal mice, and one of the two, AK23, was able to induce the PV phenotype when hybridoma cells were inoculated into the peritoneal cavities of Rag2$^{-/-}$ mice. The other six mAbs failed to show apparent pathogenic activity, in spite of their ability to bind the native Dsg3 *in vivo*.

In the present study, we isolated a further 10 anti-Dsg3 IgG mAbs from PV model mice that received naive Dsg3$^{-/-}$ splenocytes (NAK series). We characterized the pathogenic activities of these mAbs in three different assays (passive transfer, ascites formation, and *in vitro* dissociation), and also analyzed their conformational epitopes. We found that anti-Dsg3 mAbs reacting with different parts of the molecule are synergistic in their pathogenic activity, inducing blister formation when they are combined.

RESULTS

Production of NAK anti-Dsg3 IgG mAbs from PV model mice

As a source of hybridoma cells, we used splenocytes of PV model mice generated by adoptive transfer of splenocytes from naive Dsg3$^{-/-}$ mice, which produce more potent anti-Dsg3 IgG antibodies than mice receiving immunized Dsg3$^{-/-}$ splenocytes (Aoki-Ota *et al.*, 2004). We first screened the hybridoma cells by ELISA against recombinant mouse Dsg3; positive clones were further screened by live staining of mouse keratinocyte PAM212 cells. The second screening selected mAbs that could bind to the native Dsg3 on keratinocyte cell surfaces *in vivo*. Ten independent clones were isolated and designated as NAK mAbs (Table 1).

All of the NAK mAbs had the κ isotype light chain. Four (NAK1, 2, 3, 5) had IgG1 and six (NAK4, 7, 8, 9, 10, 11) had IgG2a heavy chains (Table 1). Under indirect immunofluorescence, all stained keratinocyte cell surfaces in all layers of the mouse oral mucosa, with stronger intensity toward the more basal layers (Figure 1, mouse hard palate and see also Supplementary Figure 1) and in the basal and parabasal layers of the mouse epidermis (Figure 1, mouse tail skin). Five mAbs (NAK1, 4, 7, 8, 9) also stained the keratinocyte cell surfaces of human epidermis, but with different staining patterns. NAK1 and NAK9 mAbs stained the lower layers of the human epidermis, NAK4 stained all layers, and NAK7 and NAK8 stained the middle to upper layers (Figure 1, human epidermis). With ELISA, all of the mAbs reacted only with mouse Dsg3 and not with mouse Dsg1. Those mAbs that showed crossreactivity with human epidermis

Table 1. Characterization of the NAK mAbs

				ELISA							Pathogenic activity		
		IIF[1]		Mouse		Human[2]		Live keratinocyte staining	Ca dependency[3]	Epitopes[4]	Passive transfer[5]	Ascites formation	Dissociation assay[6]
NAK	Isotype	Mouse	Human	Dsg3	Dsg1	Dsg3	Dsg1						
1	IgG1κ	+	+	+	–	+	–	+	+	T25, Y28, Q29	+	–	14.6
2	IgG1κ	+	–	+	–	–	–	+	+	195–402	+	–	25.2
3	IgG1κ	+	–	+	–	+	–	+	–	403–565	–	–	0.5
4	IgG2aκ	+	+	+	–	+	+	+	+	1–162	+	–	35.9
5	IgG1κ	+	–	+	–	–	–	+	–	195–402	–	–	12.5
7	IgG2aκ	+	+	+	–	–	+	+	+	1–162	+	–	13.4
8	IgG2aκ	+	+	+	–	–	+	+	+	1–162	+	–	25.4
9	IgG2aκ	+	+	+	–	+	–	+	+	T25, Y28, Q29, V53 D54, K55, N56	+	–	45.1
10	IgG2aκ	+	–	+	–	–	–	+	+	1–162	+	–	34.9
11	IgG2aκ	+	–	+	–	–	–	+	+	1–402	+	–	33.6

IIF, indirect immunofluorescence.
[1]Indirect immunofluorescence staining. Mouse oral mucosa (hard palate) and human normal skin were used as the substrates.
[2]ELISA reactivity against human Dsgs was determined with 0.1 μg/ml NAK mAbs.
[3]The reactivity of NAK mAbs against mouse Dsg3 was determined with or without EDTA treatment. +, indicates the abolition of the reactivity by EDTA.
[4]The epitopes are indicated by the residue numbers for mouse Dsg3 except those for NAK1 and NAK9 mAbs, whose epitopes are indicated by the residues for human Dsg3.
[5]+, indicates gross blister formation when coinjected with PF IgG.
[6]Dissociation index values are listed when dissociation index obtained by AK23 mAb (Tsunoda *et al.*, 2003) is 100.

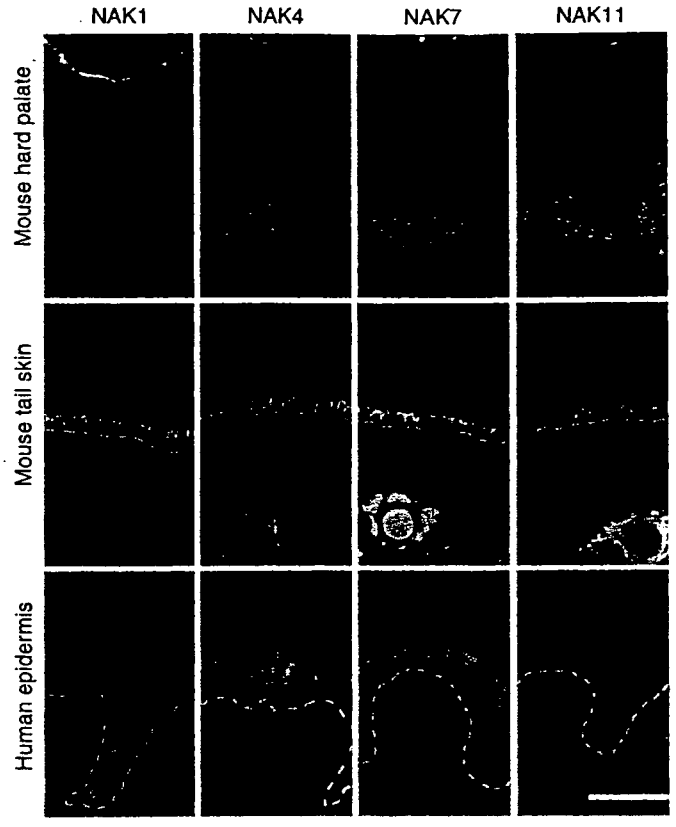

Figure 1. Immunostaining of mouse and human tissues with NAK mAbs. Representative immunostaining is shown (NAK1, NAK4, NAK7, and NAK11). All of the NAK mAbs stained keratinocyte cell surfaces in all layers of mouse oral mucosa (mouse hard palate), with stronger intensity toward the lower layers, and stained the lower layers of mouse epidermis (mouse tail skin), where Dsg3 is expressed. NAK mAbs reacted with human epidermis in different patterns (human epidermis); NAK1, NAK4, and NAK7 mAbs stained the lower portion of, the entire, and the upper portion of human epidermis, respectively, while NAK11 failed to react with human epidermis. Dashed lines indicate the basement membrane zone. Bar = 50 μm.

under immunofluorescence also recognized human Dsg3 and/or Dsg1 in different patterns. NAK1, NAK3, and NAK9 reacted with human Dsg3, NAK4 reacted with both human Dsg3 and Dsg1, and NAK7 and NAK8 reacted with human Dsg1 (Table 1). The immunofluorescence staining patterns of NAK mAbs whose IIF was positive on human epidermis (NAK1, 4, 7, 8, 9) were consistent with the ELISA results, based on the distribution of Dsg1 and Dsg3 in the human epidermis (Amagai *et al.*, 1996; Shirakata *et al.*, 1998).

Thus, all NAK mAbs specifically reacted with native mouse Dsg3 without crossreacting with mouse Dsg1, and some crossreacted with human Dsg3 and/or Dsg1 in different patterns.

NAK mAbs recognize different epitopes on Dsg3

To characterize the epitopes of the NAK mAbs, we determined whether their binding to mouse Dsg3 was dependent on calcium. Treating a mouse Dsg3-coated ELISA plate with EDTA did not substantially alter binding of NAK3 and NAK5, but abolished binding of the other mAbs (data not shown). Therefore, NAK3 and NAK5 mAbs recognized Ca^{2+}-independent epitopes, while the other mAbs recognized Ca^{2+}-dependent conformational epitopes.

To map the epitopes of the mAbs, we used domain-swapped mouse Dsg3/Dsg1 recombinant molecules (Anzai *et al.*, 2004). These molecules are believed to maintain native conformations, at least in terms of binding anti-Dsg IgG antibodies (Futei *et al.*, 2000; Sekiguchi *et al.*, 2001). We used four domain-swapped molecules that contained the mouse Dsg3 residues 1–162 ($mDsg3^{1-162}/mDsg1^{163-512}$), 1–402 ($mDsg3^{1-402}/mDsg1^{403-512}$), 195–565 ($mDsg1^{1-194}/mDsg3^{195-565}$), or 403–565 ($mDsg1^{1-402}/mDsg3^{403-565}$). NAK1, 4, 7, 8, 9, 10 mAbs precipitated residues 1–162 and 1–402, but not residues 195–565 or 403–565 (Figure 2a and b). Their epitopes appear to reside in residues 1–162, the N-terminal portion of the extracellular domain of mouse Dsg3. NAK2 and NAK5 reacted with residues 1–402 and 195–565, but not with residues 1–162 or 403–565 (Figure 2a and b). Their epitopes appear to be in residues 195–402, which represent the middle portion of the extracellular domain. NAK3 precipitated residues 195–565 and 403–565, but not residues 1–162 or 1–402 (Figure 2a and b). Its epitope appears to reside in residues 403–565, the C-terminal portion of the extracellular domain. NAK11 mAb precipitated only residues 1–402 (Figure 2a and b).

Of these mAbs, NAK1 and NAK9 crossreacted with human Dsg3 but not with human Dsg1, and recognized the N-terminal residues 1–162. We used a series of point-mutated human Dsg3 and Dsg1 molecules, in which Dsg3-specific residues were replaced by the corresponding Dsg1-specific residues, or *vice versa* (Figure 2d; Tsunoda *et al.*, 2003). NAK1 mAb maintained its reaction with human Dsg3 mutated at T31, K33, I34 (Dsg3-M2), V53-N56 (Dsg3-M3), E70, S73 (Dsg3-M4), L75, T77 (Dsg3-M5), A83, and Q84 (Dsg3-M6), but lost reactivity when the Dsg3 specific residues T25, Y28, or Q29 were mutated (Dsg3-M1, M1-2, M1-2-3) (Figure 2c and d). NAK1 gained recognition of human Dsg1 modified with Dsg3-specific residues at T25, Y28, or Q29 (Dsg1-M1-2, M1-2-3) (Figure 2c and d). These findings indicate that the epitope for NAK1 maps to the T25, Y28, and Q29 of Dsg3. T25 and Q29 are conserved between human and mouse Dsg3, but Y28 in the human is replaced by F28 in the mouse.

Similarly, NAK9 mAb reacted with human Dsg3 mutated at Dsg3-specific residues T31, K33, I34 (Dsg3-M2), E70, S73 (Dsg3-M4), L75, T77 (Dsg3-M5), A83, and Q84 (Dsg3-M6), but lost recognition when either T25, Y28, Q29 (M1), or V53-N56 (Dsg3-M3) were mutated (Figure 2c and d). NAK9 gained recognition of human Dsg1 when mouse residues T25, Y28, Q29, and V53-N56 were introduced (Dsg1-M1-2-3), but not when T25, Y28, and Q29 were introduced with T31, K33, and I34 (Dsg1-M1-2) (Figure 2c and d). These findings indicate that the epitope of NAK9 mAb maps to the residues T25, Y28, Q29, V53, D54, K55, and N56. Of these, Y28 and K55 are not conserved in mouse Dsg3 (F28, P55).

Thus, these NAK mAbs recognize different epitopes on Dsg3, and six of them recognize the N-terminal 1–162 residues (Table 1).

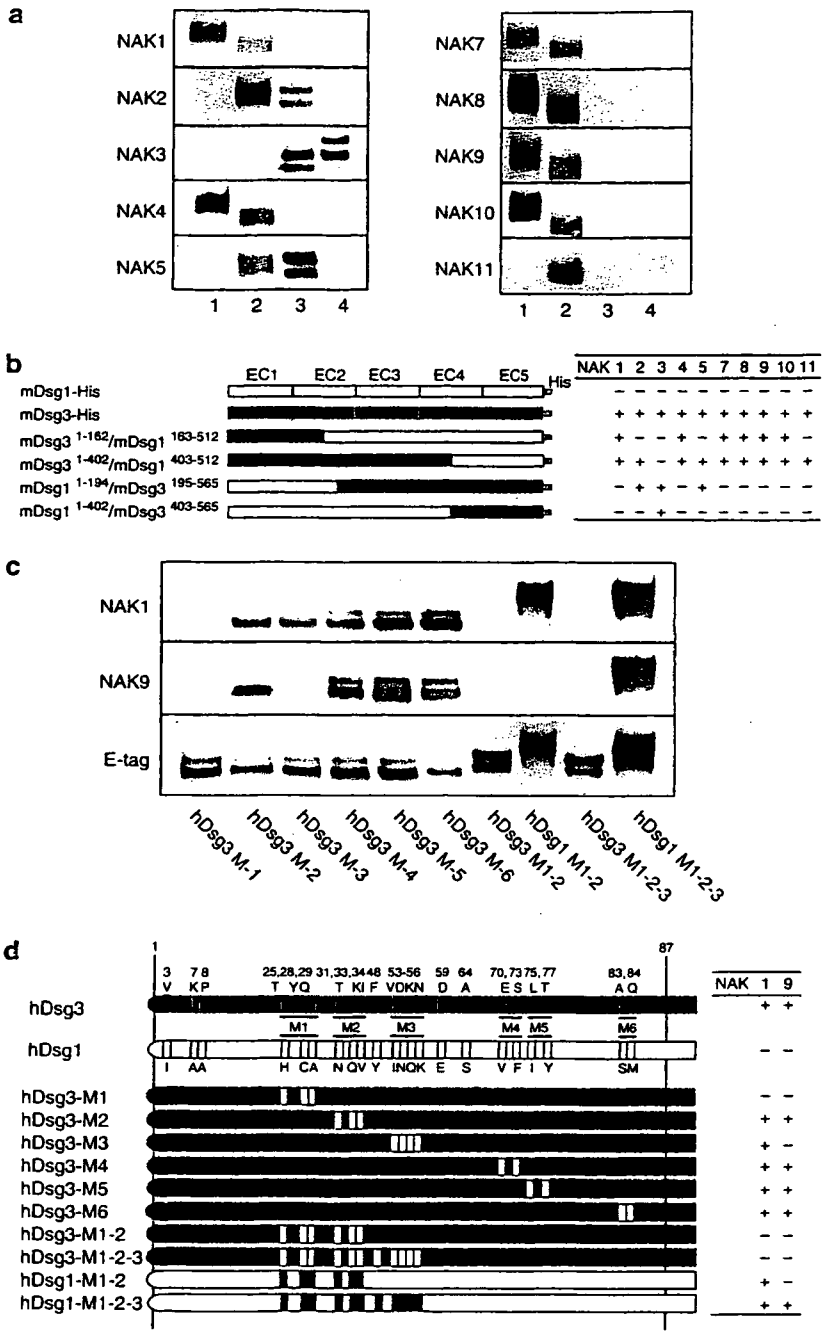

Figure 2. Immunoprecipitation of domain-swapped and point-mutated Dsg1/Dsg3 recombinant proteins with NAK mAbs. (a) Immunoprecipitation of mDsg3$^{1-162}$/mDsg1$^{163-512}$ (lane 1), mDsg3$^{1-402}$/mDsg1$^{403-512}$ (lane 2), mDsg1$^{1-194}$/mDsg3$^{195-596}$ (lane 3), and mDsg1$^{1-402}$/mDsg3$^{403-565}$ (lane 4) with various NAK mAbs. (b) The molecular structure of domain-swapped mDsg1/mDsg3 proteins and summary of results for epitope mapping of mAbs. (c) Immunoprecipitation of various point-mutated hDsg1/hDsg3 proteins with NAK1 (upper panel), NAK9 (middle panel), and anti-E-tag mAb as a positive control (lower panel). (d) The molecular structure of point-mutated hDsg1/hDsg3 proteins and summary of results for epitope mapping of NAK1 and NAK9 mAbs. The 22 amino-acid residues not conserved between hDsg1 and hDsg3 are indicated. These nonconserved residues were switched between Dsg1 and Dsg3 to generate point-mutated molecules.

Most NAK mAbs induce blisters in passive transfer to neonatal mice

To evaluate the pathogenic activities of the mAbs, we first performed a passive transfer assay using neonatal mice, a well-established assay for pemphigus (Anhalt *et al.*, 1982; Amagai *et al.*, 1994). Purified IgG from the culture supernatant of each hybridoma was injected s.c. into neonatal mice, and the mice were observed for 18–24 hours postinjection (Table 2). When individual NAK mAbs were injected, none of them induced gross blistering; this was expected, as

Dsg1 co-expression in the skin of neonatal mice compensates for the impaired adhesive function of Dsg3 (Figure 3; Amagai, 1999; Mahoney *et al.*, 1999). However, all of the mAbs except NAK3 induced varying degrees of microscopic blistering, with histological evidence of suprabasilar acantholysis (Figure 3). We scored the extent of this blistering using the total area of blisters observed in histology (Table 2).

To overcome the compensation by Dsg1, we used IgG prepared from pemphigus foliaceus (PF) sera that contained anti-Dsg1 IgG autoantibodies. We injected one-half of the minimum dose of PF IgG that had been shown to induce gross blisters, alone or in combination with NAK mAbs (Tsunoda *et al.*, 2003). Neonatal mice that were co-injected with each of the NAK mAbs (except NAK3 and NAK5) developed extensive gross blisters with suprabasilar acantholysis, while mice injected with the PF IgG alone did not show any blister formation (Figure 3).

These findings indicate that most of the NAK mAbs are able to induce the loss of cell–cell adhesion of keratinocytes in neonatal mice. Only two failed to show pathogenic effects.

Table 2. Summary of the pathogenic activities of NAK mAbs in passive transfer assay

	NAK alone[1]			NAK+PF IgG[2]	
			Blister formation		
NAK	*n*	IgG deposition	Histologic blister Scores[3]	*n*	Gross blisters
1	3	+	5.70	3	3
2	3	+	16.31	2	2
3	3	+	0	2	0
4	3	+	38.91	3	1
5	3	+	4.04	2	0
7	3	+	4.82	2	2
8	3	+	6.38	2	2
9	3	+	22.23	2	2
10	3	+	4.77	4	2
11	3	+	9.48	2	2

PF, pemphigus foliaceus.
[1]NAK mAbs alone were subcutaneously injected into neonatal mice and the formation of gross or microscopic blisters was noted.
[2]NAK mAbs were coinjected with 50% of the minimum dose of PF IgG into neonatal mice and the formation of gross blisters was noted. The number of mice with the gross blisters was listed.
[3]The blister score is defined in Materials and Methods.

None of the individual NAK mAbs induce the PV phenotype in adult mice

To further evaluate the pathogenic activities of NAK mAbs, we inoculated individual hybridoma cells intraperitonealy into $Rag2^{-/-}$ immunodeficient mice (6–8 weeks old), and looked for the appearance of the PV phenotype, which includes weight loss, patchy hair loss, and mucosal erosions (Figure 4, Table 3). None of the recipient mice developed this phenotype, even after obvious ascites fluid formation at day 15. Although all the mice showed *in vivo* IgG deposition on keratinocyte cell surfaces of the skin and mucous membranes, no blister formation was apparent in the oral mucosa at the histological level (Figure 4).

These findings indicate that none of the individual NAK clones inoculated was potent enough to induce the loss of cell–cell adhesion of keratinocytes *in vivo*, during ascites formation in adult mice.

Combined NAK mAbs induce the PV phenotype in adult mice

To explore the possibility of combined pathogenic effects, we inoculated NAK hybridoma cells intraperitonealy in various combinations into $Rag2^{-/-}$ mice (Figure 4, Table 3). When hybridoma cells for NAK1, 2, 4, 7, 8, 9, 10, and 11 were combined, the recipient mice developed weight loss, patchy hair loss, and crusted erosions around the snout, at approximately days 10–15 after the inoculation. These mice showed suprabasilar acantholysis of the oral mucosa and in the skin around the snout, together with *in vivo* IgG deposition on keratinocyte surfaces. The titers of circulating anti-Dsg3 IgG in the recipient mice with combined NAK hybridoma cells were compatible with those with single NAK hybridoma cells. The development of the PV phenotype was observed even after mAbs NAK8, NAK4, NAK10, and NAK9 were sequentially removed from the combination (Table 3). The minimum combination that was sufficient to induce the PV phenotype in all recipient mice tested was NAK1, NAK2, NAK7, and NAK11, or NAK2, NAK3, NAK5, and NAK11,

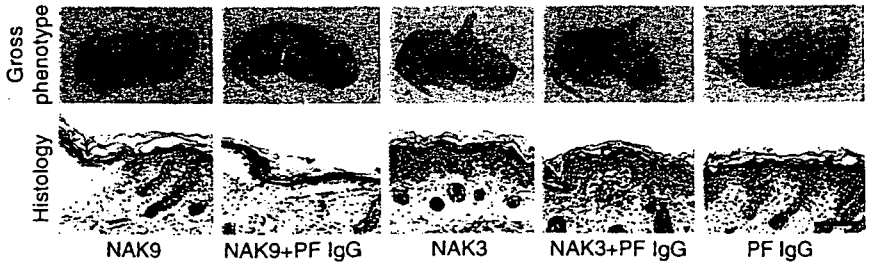

Figure 3. Passive transfer assay of NAK mAbs in neonatal mice. All antibodies except NAK3 and NAK5 mAbs (which recognize Ca^{2+}-independent epitopes) induced gross PV blisters when co-injected with a dose of PF IgG insufficient to induce blisters on its own. Representative data are shown. Neonatal mice injected with NAK9, but not with NAK3, developed microscopic blisters with histological suprabasilar acantholysis, without apparent gross blisters. Neonatal mice co-injected with NAK9, but not NAK3 or PF IgG alone, developed extensive blistering (arrows) with suprabasilar acantholysis. Bar = 50 μm.

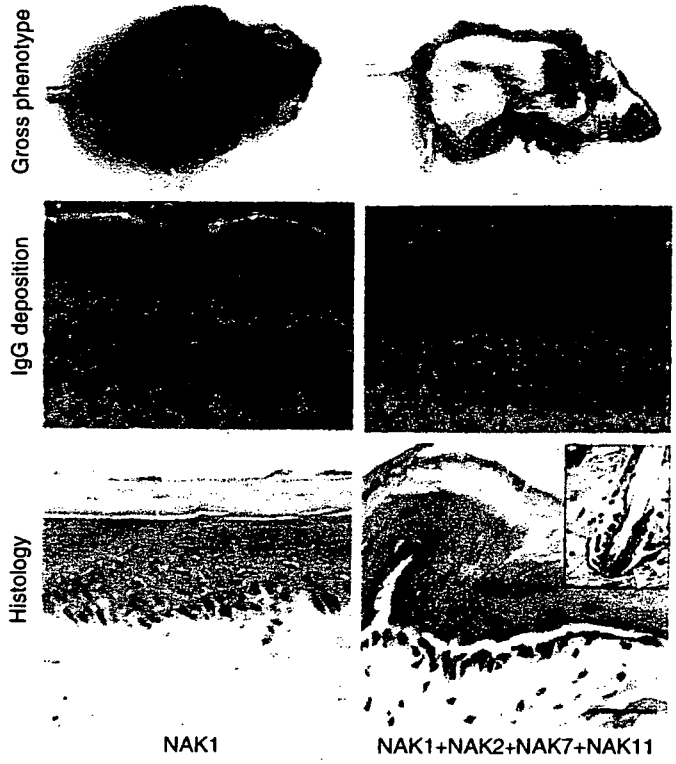

Figure 4. Combinations of NAK mAbs induced the PV phenotype when their hybridoma cells were inoculated intraperitonealy, while the individual mAbs failed to do so. Mice inoculated with NAK1 hybridoma cells alone did not develop apparent PV phenotype (day 15 after inoculation) or histological suprabasilar acantholysis, in spite of apparent ascites formation and *in vivo* IgG deposition on keratinocyte cell surfaces of stratified squamous epithelia. In contrast, when hybridoma cells producing NAK1, NAK2, NAK7, and NAK11 mAbs were combined, recipient mice developed patchy hair loss as well as weight loss (day 15). Histology of the oral mucosa showed *in vivo* IgG deposition and suprabasilar acantholysis and the skin showed acantholysis around telogen hair club (inset; arrow heads indicate the location of acantholysis). Bar = 50 μm.

Table 3. Summary of the pathogenic activities of NAK mAbs in ascites formation assays

NAK	*n*	IgG deposition[1]	PV phenotype[2] (*n* (%))	Titers of circulating anti-Dsg3 IgG[3]
1	7	+	0	144.2±9.3
2	4	+	0	72.9±1.3
3	10	+	0	230.6±38.9
4	5	+	0	ND
5	11	+	0	181.0±20.0
7	3	+	0	92.0±1.0
8	4	+	0	85.3±1.3
9	8	+	0	111.6±4.2
10	8	+	0	41.1±3.3
11	6	+	0	ND
1,2,4,7,8,9,10,11	5	+	5 (100)	114.0±14.7
1,2,4,7,9,10,11	3	+	3 (100)	113.6±0.1
1,2,7,9,11	2	+	2 (100)	ND
1,2,7,11	7	+	7 (100)	126.5±5.9
2,3,5,11	3	+	3 (100)	219.3±5.9
2,7,11	3	+	2 (67)	77.2±6.7
1,2,11	4	+	2 (50)	112.1±2.8
1,2,7	4	+	0	218.3±5.9
1,7,11	4	+	0	175.5±13.0
2,3,5	3	+	0	208.8±5.9
2,11	3	+	1 (33)	55.7±5.6
2,7	2	+	0	94.1±21.5
7,11	3	+	0	ND

ND, not determinded; PV, pemphigus vulgaris.
Hybridoma cells for individual NAK clones or combinations were inoculated intraperitonealy into Rag2$^{-/-}$ mice.
[1]IgG deposition on mouse keratinocyte cell surfaces was observed in all mice injected with NAK mAb hybridomas.
[2]The development of the PV phenotype, including patchy hair loss and suprabasilar acantholysis of the oral mucosa, was evaluated. The number of mice with the PV phenotype was listed.
[3]Titers of circulating anti-Dsg3 IgG were measured by mDsg3 ELISA at days 15–20 days after inoculation.

each of which recognize different epitopes on mouse Dsg3 (Table 1). The mice inoculated with hybridoma cells from these clones developed the full spectrum of PV phenotypic markers (Figure 4).

When we removed any NAK hybridoma cells from the above minimum combination, some of the recipient mice started not to develop the PV phenotype and the other mice showed the PV phenotype at approximately days 15–20 after the inoculation (Table 3). The minimum combination that could induced the PV phenotype at least one of the mice tested was NAK2 and NAK11 hybridoma cells (Table 3).

These findings indicate that NAK mAbs that are not sufficient to induce blisters singly are capable of doing so in adult mice when they are combined.

Pathogenic ranking of NAK mAbs by *in vitro* dissociation assay

The passive transfer assay with neonatal mice and the ascites formation assay with Rag2$^{-/-}$ adult mice require relatively large amounts of antibodies, and do not necessarily simulate pathogenesis in a quantitative fashion. We recently developed an *in vitro* dissociation assay using primary cultures of normal human keratinocytes, as a simple method to quantify the pathogenic strength of pemphigus autoantibodies (Ishii *et al.*, 2005). For this study, we modified the assay to evaluate the pathogenic activity of NAK mAbs against mouse keratinocytes. To obtain Dsg3-dominated cell–cell adhesion, we used primary cultured mouse keratinocytes, which express a low level of Dsg2, in the presence of exfoliative toxin A, which specifically digests Dsg1 (Amagai *et al.*, 2000a). After incubation with various NAK mAbs, a sheet of keratinocytes, released by dispase, were subjected to mechanical stress by pipetting, and the number of cell sheet fragments was determined. The number of cell fragments

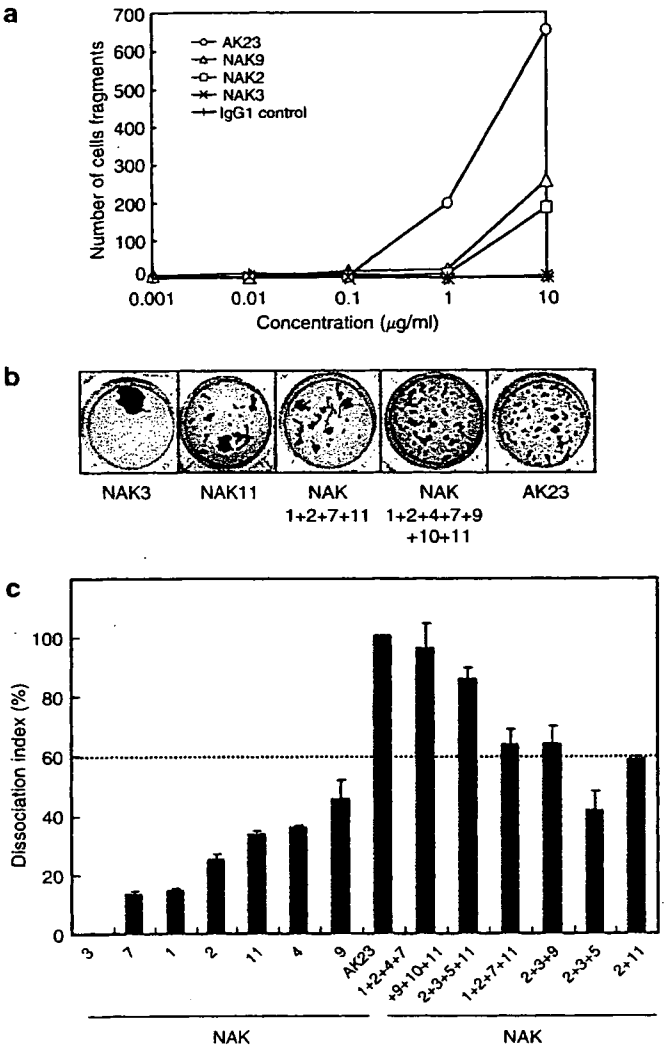

Figure 5. *In vitro* keratinocyte dissociation assays demonstrated synergistic pathogenic effects of NAK mAbs in the loss of keratinocyte cell–cell adhesion. Sheets of mouse keratinocytes were treated with exfoliative toxin A to digest Dsg1and with NAK mAbs, and subjected to mechanical stress. Cell fragments were counted by image analysis. Representative data are shown. (**a**) Dose dependency of NAK mAbs on dissociation scores. (**b**) NAK11 induced fragmentation while NAK3 did not. The combined mAbs generated similar numbers of cell fragments as did AK23, an anti-Dsg3 mAb that is able to induce the PV phenotype (Tsunoda *et al.*, 2003). (**c**) Dissociation indexes of NAK mAbs alone and in combination. The dissociation index varied among the mAbs. Combinations of mAbs (adjusted to 1 μg/ml) had higher dissociation indexes than individual NAK mAbs. Combining these data with the results from ascites formation assays indicates that the threshold for blister formation *in vivo* may be at a dissociation index of approximately 60% (dashed line).

increased as the concentration of AK23 or various NAK mAbs increased, indicating that this assay evaluate pathogenic strength in a quantitative manner (Figure 5a). Dissociation index values were calculated as a percent of the number of fragments obtained with a positive control mAb, AK23 (Tsunoda *et al.*, 2003).

Each NAK mAb had a different dissociation index, indicating that this assay could discriminate differences in activity among them (Table 1, representative data are shown in Figure 5b and c). NAK3 and NAK5, which failed to induce apparent pathogenic activity in the passive transfer model, gave smaller dissociation indexes than the others (0.5 and 12.5%, respectively), while NAK9 had the highest dissociation index (45.1%).

When several NAK mAbs were combined, without changing the total amount of IgG added (1 μg/ml), dissociation scores greatly increased (Figure 5c). When NAK1, 2, 4, 7, 9, 10, and 11 mAbs were combined, the dissociation score was equivalent to that of the AK23 mAb, hybridoma cells of which can alone induce the PV phenotype in adult mice (Tsunoda *et al.*, 2003). When we removed some of NAK mAbs from the combination, the dissociation scores gradually decreased in general. The dissociation scores of the all combinations were still higher than those of the individual NAK mAbs, indicating a synergistic pathogenic effect (representative data in Figure 5c). Considering these results with those of the ascites formation assay, we speculate that there may be a threshold of blister formation *in vivo* in adult mice corresponding to a dissociation index of approximately 60% (dashed line in Figure 5c).

These findings indicate that individual NAK mAbs have various pathogenic activities in disrupting the cell–cell adhesion mediated by Dsg3, none individually potent enough to induce an apparent PV phenotype in adult mice. However, combinations of these mAbs show synergistic effects above the threshold for blister formation and development of the PV phenotype.

DISCUSSION

In this study, we generated 10 anti-Dsg3 IgG mAbs from PV model mice produced by adoptive transfer of naive Dsg3$^{-/-}$ splenocytes. All mAbs specifically reacted with native mouse Dsg3, but not with mouse Dsg1. Some (NAK1, 3, 4, 7, 8, 9) cross-reacted with human Dsgs, although the isoform specificities of the mAbs were not necessarily conserved between mouse and human. NAK1, NAK3, and NAK9 reacted only with human Dsg3, while NAK4 reacted with both human Dsg3 and Dsg1, and NAK7 and NAK8 reacted only with human Dsg1. These findings indicate that antibodies against Dsgs have fine specificities, determined by the few amino-acid residues that are not conserved between mouse and human isoforms. This highlights the difficulty of performing detailed evaluations of these mouse antibodies using human skin or keratinocytes and *vice versa*.

We performed three different assays to evaluate the pathogenic activities of NAK mAbs: passive transfer, ascites formation, and *in vitro* dissociation. The passive transfer assay, by injection of IgG into neonatal mice, is well established (Anhalt *et al.*, 1982), and the ascites formation assay, after inoculation of hybridoma cells into immunodeficient adult mice, has been developed to evaluate *in vivo* pathogenic activity of anti-Dsg3 mAbs (Tsunoda *et al.*, 2003). The passive transfer assay is more easily controlled than the ascites formation assay. Highly concentrated IgG can be applied to neonatal mice by passive transfer, while the

amount of IgG in an ascites formation assay is dependent on the production rate of the hybridoma cells. Although these two assays reflect *in vivo* pathogenic activity of anti-Dsg3 IgG and subjective scaling can be used to represent the extent of the phenotypic results (Mahoney *et al.*, 1999; Aoki-Ota *et al.*, 2004), these assays do not measure pathogenic strength in a quantitative manner. To compare pathogenic strengths among pemphigus sera or anti-Dsg3 IgG mAbs, an *in vitro* dissociation assay was developed using primary cultures of human keratinocytes (Ishii *et al.*, 2005). In this study, we modified that assay using mouse keratinocytes to analyze the potential of each NAK mAb.

Under passive transfer, eight of 10 mAbs showed pathogenic activity and induced blister formation (Figure 3, Tables 1 and 2), while only two of eight AK mAbs, isolated from PV model mice receiving immunized $Dsg3^{-/-}$ splenocytes, were pathogenic (Tsunoda *et al.*, 2003). The higher frequency of pathogenicity among NAK mAbs is consistent with the fact that although mice receiving naive $Dsg3^{-/-}$ splenocytes showed lower titers of anti-Dsg3 IgG than did those receiving immunized splenocytes, the two types of mice showed no apparent differences in disease severity (Aoki-Ota *et al.*, 2004). The eight pathogenic NAK mAbs recognized Ca^{2+}-dependent epitopes on Dsg3, while the epitopes of the two nonpathogenic NAK mAbs were not dependent on Ca^{2+} (Table 1). Similar results have been seen with the AK mAbs: the two pathogenic antibodies were dependent on Ca^{2+}, while the six nonpathogenic AK mAbs were independent of Ca^{2+} (Tsunoda *et al.*, 2003). Most of pemphigus patients' IgG autoantibodies recognize Ca^{2+}-dependent epitopes on Dsg3 (Matis *et al.*, 1987; Eyre and Stanley, 1988; Amagai *et al.*, 1995). These findings together strongly suggest that pathogenic antibodies recognize Ca^{2+}-dependent conformational epitopes while nonpathogenic antibodies react with Ca^{2+}-independent linear epitopes.

Although eight of 10 NAK mAbs showed pathogenic activity in the passive transfer assay, none induced the PV phenotype in the ascites formation assay (Figure 4, Table 1), indicating that none were as potent as mAb AK23, which could induce the PV phenotype in adult mice upon hybridoma inoculation (Tsunoda *et al.*, 2003). More sensitive in vitro dissociation assays confirmed this and allowed us to rank the pathogenicity of NAK mAbs (Figure 5). In fine mapping using human Dsg1/Dsg3 point-mutated molecules, the epitopes of NAK 1 and 9, which crossreacted with human Dsg3, were mapped, respectively, to the amino-terminal T25, Y28, and Q29 and to T25, Y28, Q29, V53-N56 of Dsg3. These residues form a part of the adhesive interface of Dsg3 as predicted by crystal structure (Boggon *et al.*, 2002), but are different from the AK23 epitope (V3, K7, P8, and D59) (Tsunoda *et al.*, 2003). These findings suggest that the residues V3, K7, P8, and D59 may form the critically important part of the adhesive interface of Dsg3.

Although our attempt to isolate pathogenic anti-Dsg3 mAbs as potent as AK23 was not successful, pemphigus patients' sera always contain polyclonal anti-Dsg3 IgG autoantibodies, which recognize different parts of the molecule (Amagai *et al.*, 1992; Sekiguchi *et al.*, 2001). We therefore tested the possibility that a combination of several weakly pathogenic mAbs might show a synergistic effect and induce the PV phenotype in adult mice. Indeed, when the combination of hybridoma cells producing NAK1, 2, 4, and 7–11 were inoculated into $Rag2^{-/-}$ mice, the recipients developed the PV phenotype, with weight loss, patchy hair loss, and crusted erosions around the snout (Table 3). The minimal combination tested that was sufficient to induce the phenotype in all mice tested was NAK1, 2, 7, and 11 mAbs or NAK2, 3, 5, 11 mAbs (Figure 4). *In vitro* dissociation assays confirmed the synergistic pathogenic effects of NAK mAbs (Figure 5). This is the first demonstration of synergism among antidesmoglein IgG antibodies in inducing the loss of cell–cell adhesion of keratinocytes *in vivo* and *in vitro*.

In a previous study, AK mAbs recognizing the middle to C-terminal extracellular domain of Dsg3 did not show apparent pathogenic activity, suggesting that IgGs reacting with functionally less important parts of the molecule do not contribute to pathogenesis (Tsunoda *et al.*, 2003). However, in this study, NAK mAbs recognizing such regions showed synergistic effects with mAbs reacting with the N-terminal domain (e.g., mAbs NAK2, 3, and 9 or NAK2 and 11 in Figure 5c, Table 3). These findings provide molecular evidence that anti-desmoglein IgG antibodies recognizing the middle to C-terminal extracellular domains of Dsg3 can also take part in the pathogenic process of blister formation.

We knew that the dose of antibodies is an important factor to determine the pathogenic strength of patients' sera because antibody titers are generally correlated with the disease activities when monitored in individual patients (Sams and Jordon, 1971; Ishii *et al.*, 1997; Cheng *et al.*, 2002). We also knew that the epitope of antibodies is another important factor to determine the pathogenic strength of each anti-Dsg3 IgG (Tsunoda *et al.*, 2003). In this study, we demonstrated that the combination of different anti-Dsg3 IgG autoantibodies is the third important factor because most, if not all, patients' sera contain polyclonal anti-Dsg3 IgG. Thus, the clinical severity of the disease in each patient may be determined in a more complex manner than initially thought.

The preclinical condition in patients that precedes development of PV remains to be elucidated. One possibility is that one or a few nonpathogenic or weakly pathogenic anti-desmoglein IgG autoantibody (or autoantibodies) are first generated without inducing the apparent disease; additional autoantibodies recognizing different epitopes on desmoglein are subsequently produced, with the onset of the disease phenotype. It would be interesting to study whether signal transduction induced by the combined weakly pathogenic NAK mAbs and by the single AK23 mAb are different. Also of interest is whether long-term *in vivo* binding of weakly pathogenic antibodies induces any secondary inflammation in mice, including the recruitment of eosinophils. The weakly pathogenic anti-Dsg3 NAK mAbs together with the potent AK23 mAbs provide valuable tools to replicate and study the polyclonal condition as found in patients, and to dissect the molecular pathophysiology of pemphigus.

MATERIALS AND METHODS

Mice

$Dsg3^{-/-}$ offspring were obtained from matings of homozygotes (Amagai *et al.*, 2000b; Tsunoda *et al.*, 2002). These mice had the mixed genetic background of 129/SV (H-2^b) and C57BL/6J (H-2^b). Splenocytes (5×10^7) were prepared from naive $Dsg3^{-/-}$ mice, and adoptively transferred into C57BL/6 $Rag2^{-/-}$ mice (Central Institute for Experimental Animals, Tokyo, Japan) via the tail vein, as previously described (Aoki-Ota *et al.*, 2004). Anti-Dsg3 antibody production was examined by ELISA for recombinant mouse Dsg3, and *in vivo* binding against Dsg3 was confirmed by live keratinocyte staining (Tsunoda *et al.*, 2002). All mouse studies were approved by the Animal Ethics Review Board of Keio University.

Production of NAK mAbs

Splenocytes were isolated from mice that had the active PV phenotype and fused with P3 mouse myeloma cells at a ratio of 5:1 with PEG 4000 (Merck, Darmstadt, Germany), followed by selection with hypoxanthine–aminopterin–thymidine in the presence of 10% hybridoma cloning factor (IGEN, Gaithersburg, MD). Hybridoma cells were screened by ELISA using recombinant mouse Dsg3 and positive clones were further examined by live keratinocyte staining. Ten positive clones were screened and designated as NAK (AK mAb from PV model mice by naive splenocyte transfer) (Table 1). Each clone was obtained by three replicates of the limiting dilution method. The isotypes of mAbs produced were determined using an isotyping kit (Roche Diagnostics, Mannheim, Germany). Antibodies were purified from culture supernatants using the HiTrap rProtein A FF column (Amersham Biosciences, Buckinghamshire, UK).

ELISA and live keratinocyte staining

The reactivities of antibodies with mouse Dsg3, mouse Dsg1, human Dsg3, and human Dsg1 were measured by ELISA using the respective recombinant Dsg molecules, as described previously (Amagai *et al.*, 2000b; Tsunoda *et al.*, 2003; Anzai *et al.*, 2004). In brief, each sample was diluted 50,000-fold and run in duplicate. A standard serum obtained from a $Dsg3^{-/-}$ mouse immunized with $mDsg3^{-/-}$ was used as a positive control, and serum from a nonimmunized mouse was used as a negative control. The ELISA scores were calculated as index values using the formula: index value = (OD_{450} of sample − OD_{450} of negative control)/(OD_{450} of positive control − OD_{450} of negative control) × 100. Live keratinocyte staining was performed using the mouse keratinocyte cell line PAM212, as described previously (Amagai *et al.*, 2000b; Tsunoda *et al.*, 2003). To confirm calcium sensitivity of epitopes, an EDTA-treated ELISA was performed, incubating the ELISA plate with 5mM EDTA prior to the assay.

Epitope mapping by immunoprecipitation using chimeric desmogleins

Immunoprecipitation was performed using domain-swapped or point-mutated Dsg1/Dsg3 molecules to determine mAb epitopes (Tsunoda *et al.*, 2003; Anzai *et al.*, 2004). Typically, 3 μg of purified mAb and 200 μl of culture supernatant containing recombinant protein were mixed and incubated at room temperature for 30 minutes. These proteins were immunoprecipitated with protein G-Sepharose (Amersham Biosciences) overnight at 4°C. Anti-E-tag mAb (Amersham Biosciences) was used as a positive control. The immunoprecipitates were fractionated by SDS-PAGE and blotted onto a polyvinylidene difluoride membrane (Millipore, Bedford, MA). The recombinant proteins were visualized with an anti-6x histidine Ab (R&D Systems, Minneapolis, MN).

Passive transfer assays using neonatal mice

The pathogenic activities of the mAbs were evaluated by passive transfer in neonatal mice, an established assay for the pathogenic activity of pemphigus sera (Anhalt *et al.*, 1982; Amagai *et al.*, 1994). We injected NAK mAbs (120–250 μg/mouse, the highest dose we injected per mice) either alone or together with a small amount of total IgG prepared by ammonium sulfate precipitation of PF serum. The dosage of PF IgG was set at 50% of that needed to induce gross blistering, that is, 1 mg/mouse. Neonatal ICR (Institute of Cancer Research) mice (Sankyo Lab Service, Tokyo, Japan) were used at 12–24 hours after birth (body weight 1.5–2.0 g). The skin was evaluated grossly and microscopically 18–24 hours after injection. To evaluate microscopic blisters, the entire body skin was sectioned into six strips of about 3 mm in width. Blister formation was considered positive when the length of a single lesion was greater than 120 μm or when more than two acantholytic lesions were found after examining all six sections. Blisters found at the edges of sections were not counted. To quantify the extent of blister formation histologically, we calculated scores using the following formula: histologic blister score = ((combined total length of all blistered regions)/(combined total length of all sections examined)) × 100.

Ascites formation assay

To evaluate the pathogenic activity of the NAK mAbs in adult mice, we inoculated 5×10^6–1×10^7 cells, from individual hybridomas or from a mixture of clones, into the peritoneum of $Rag2^{-/-}$ mice primed with 2,6,10,14-tetramethyl-pentadecane (Wako Pure Chemical Industries, Osaka, Japan). The inoculated mice were monitored for ascites formation as well as for the appearance of the PV phenotype, manifested by weight loss and patchy hair loss. Biopsies of the oral mucous membranes and skin were taken when mice developed the PV phenotype or when ascites formation was observed after day 14.

In vitro dissociation assay

To evaluate the activity of mAbs in the inhibition of keratinocyte cell–cell adhesion, we modified a previously described *in vitro* dissociation assay (Ishii *et al.*, 2005). For this study, we used primary cultures of mouse keratinocytes rather than human keratinocytes. For these cultures, skin specimens prepared from neonatal ICR mice at 12–24 hours of age were incubated in dispase II (Roche Diagnostics Corp., Mannheim, Germany), and separated epidermis samples were further incubated in 0.25% Trypsin (Invitrogen, Carlsbad, CA). Isolated keratinocytes were dispensed into 12-well culture plates with keratinocyte culture medium CnT-02 (CellnTec, St Gallen, Switzerland). When keratinocytes were confluent, 1.2 mM calcium was added and cells were incubated for 24 hours. Recombinant exfoliative toxin A (0.25 μg/ml) produced in *E. coli*, which specifically digests mouse Dsg1 (Amagai *et al.*, 2000a; Amagai *et al.*, 2002), was added to cultures 2 hours before the assay, in which 1 μg/ml of individual or pooled NAK mAbs (1 μg/ml total) were added to culture media. After washing with 0.9 mM Ca^{2+}-phosphate-buffered saline

twice, mouse keratinocytes were incubated with dispase II for 15 minutes to release cells as sheets. Released sheets were carefully washed twice with 0.9 mM Ca^{2+}-phosphate-buffered saline and subjected to mechanical stress by pipetting with a 1 ml disposable pipette tip. Fragments were fixed by adding formaldehyde to a final concentration of 3% and were stained with crystal violet (Sigma-Aldrich Co., St Louis, MO). A cell sheet treated with 1 μg/ml of the positive control mAb AK23 was included in each assay to adjust for inter-assay variability. The mean number of particles was determined by counting with Image Pro software (Media Cybernetics Inc., Silver Spring, MD), using three sets of digital images captured for each plate. Dissociation scores were calculated from the number of fragments (*N*) as follows: Dissociation score = ((*N* with mAb − *N* without mAb)/(*N* with AK23 − *N* without mAb)) × 100.

CONFLICT OF INTEREST

The authors state no conflict of interest.

ACKNOWLEDGMENTS

We thank Dr Shoichiro Tsukita for the mouse myeloma P3 cells and for technical advice on the development of mAbs and Dr Takeji Nishikawa for critical discussion. We also thank Ms Yoshiko Fujii for the preparation of recombinant proteins, Ms Minae Suzuki for the immunofluorescence staining and Ms Hiromi Itoh for excellent animal care. This work was supported by Grants-in-Aid for Scientific Research from the Ministry of Education, Culture, Sports, Science and Technology of Japan; the Health and Labour Sciences Research Grants for Research on Measures for Intractable Diseases; the Ministry of Health, Labor and Welfare of Japan; and Keio Gijuku Academic Development Funds.

SUPPLEMENTARY MATERIAL

Figure 1. Immunostaining of mouse and human tissues with NAK mAbs that were not listed in Figure 1.

REFERENCES

Amagai M (1996) Pemphigus: autoimmunity to epidermal cell adhesion molecules. *Adv Dermatol* 11:319–52

Amagai M (1999) Autoimmunity against desmosomal cadherins in pemphigus. *J Dermatol Sci* 20:92–102

Amagai M (2003) Pemphigus. In: *Dermatology* (Bolognia J, Jorizzo J, Rapini R, Horn TD, Mascaro J, Mancini AJ, Salasche SJ, Saurat JH, Stingl G, eds), London: Harcourt Health Sciences, 449–62

Amagai M, Hashimoto T, Shimizu N, Nishikawa T (1994) Absorption of pathogenic autoantibodies by the extracellular domain of pemphigus vulgaris antigen (Dsg3) produced by baculovirus. *J Clin Invest* 94:59–67

Amagai M, Ishii K, Hashimoto T, Gamou S, Shimizu N, Nishikawa T (1995) Conformational epitopes of pemphigus antigens (Dsg1 and Dsg3) are calcium dependent and glycosylation independent. *J Invest Dermatol* 105:243–7

Amagai M, Karpati S, Prussick R, Klaus-Kovtun V, Stanley JR (1992) Autoantibodies against the amino-terminal cadherin-like binding domain of pemphigus vulgaris antigen are pathogenic. *J Clin Invest* 90:919–26

Amagai M, Klaus-Kovtun V, Stanley JR (1991) Autoantibodies against a novel epithelial cadherin in pemphigus vulgaris, a disease of cell adhesion. *Cell* 67:869–77

Amagai M, Koch PJ, Nishikawa T, Stanley JR (1996) Pemphigus vulgaris antigen (Desmoglein 3) is localized in the lower epidermis, the site of blister formation in patients. *J Invest Dermatol* 106:351–5

Amagai M, Matsuyoshi N, Wang ZH, Andl C, Stanley JR (2000a) Toxin in bullous impetigo and staphylococcal scalded skin syndrome targets desmoglein 1. *Nat Med* 6:1275–7

Amagai M, Nishikawa T, Nousari HC, Anhalt GJ, Hashimoto T (1998) Antibodies against desmoglein 3 (pemphigus vulgaris antigen) are present in sera from patients with paraneoplastic pemphigus and cause acantholysis *in vivo* in neonatal mice. *J Clin Invest* 102:775–82

Amagai M, Tsunoda K, Suzuki H, Nishifuji K, Koyasu S, Nishikawa T (2000b) Use of autoantigen knockout mice to develop an active autoimmune disease model of pemphigus. *J Clin Invest* 105:625–31

Amagai M, Yamaguchi T, Hanakawa Y, Nishifuji K, Sugai M, Stanley JR (2002) Staphylococcal exfoliative toxin B specifically cleaves desmoglein 1. *J Invest Dermatol* 118:845–50

Anhalt GJ, Labib RS, Voorhees JJ, Beals TF, Diaz LA (1982) Induction of pemphigus in neonatal mice by passive transfer of IgG from patients with the disease. *N Engl J Med* 306:1189–96

Anzai H, Fujii Y, Nishifuji K, Aoki-Ota M, Ota T, Amagai M *et al.* (2004) Conformational epitope mapping of antibodies against desmoglein 3 in experimental murine pemphigus vulgaris. *J Dermatol Sci* 35:133–42

Aoki-Ota M, Tsunoda K, Ota T, Iwasaki T, Koyasu S, Amagai M *et al.* (2004) A mouse model of pemphigus vulgaris by adoptive transfer of naive splenocytes from desmoglein 3 knockout mice. *Br J Dermatol* 151:346–54

Boggon TJ, Murray J, Chappuis-Flament S, Wong E, Gumbiner BM, Shapiro L (2002) C-cadherin ectodomain structure and implications for cell adhesion mechanisms. *Science* 296:1308–13

Cheng SW, Kobayashi M, Tanikawa A, Kinoshita-Kuroda K, Amagai M, Nishikawa T (2002) Monitoring disease activity in pemphigus with enzyme-linked immunosorbent assay using recombinant desmoglein 1 and 3. *Br J Dermatol* 147:261–5

Eyre RW, Stanley JR (1988) Identification of pemphigus vulgaris antigen extracted from normal human epidermis and comparison with pemphigus foliaceus antigen. *J Clin Invest* 81:807–12

Futei Y, Amagai M, Sekiguchi M, Nishifuji K, Fujii Y, Nishikawa T (2000) Conformational eptiope mapping of desmoglein 3 using domain-swapped molecules in pemphigus vulgaris. *J Invest Dermatol* 115:829–34

Ishii K, Amagai M, Hall RP, Hashimoto T, Takayanagi A, Gamou S *et al.* (1997) Characterization of autoantibodies in pemphigus using antigen-specific ELISAs with baculovirus expressed recombinant desmogleins. *J Immunol* 159:2010–7

Ishii K, Harada R, Matsuo I, Shirakata Y, Hashimoto K, Amagai M (2005) *In vitro* keratinocyte dissociation assay for evaluation of the pathogenicity of anti-desmoglein 3 IgG autoantibodies in pemphigus vulgaris. *J Invest Dermatol* 124:939–46

Koch PJ, Mahoney MG, Ishikawa H, Pulkkinen L, Uitto J, Shultz L *et al.* (1997) Targeted disruption of the pemphigus vulgaris antigen (desmoglein 3) gene in mice causes loss of keratinocyte cell adhesion with a phenotype similar to pemphigus vulgaris. *J Cell Biol* 137: 1091–102

Mahoney MG, Wang Z, Rothenberger KL, Koch PJ, Amagai M, Stanley JR (1999) Explanation for the clinical and microscopic localization of lesions in pemphigus foliaceus and vulgaris. *J Clin Invest* 103:461–8

Matis WL, Anhalt GJ, Diaz LA, Rivitti EA, Martins CR, Berger RS (1987) Calcium enhances the sensitivity of immunofluorescence for pemphigus antibodies. *J Invest Dermatol* 89:302–4

Sams WMJ, Jordon RE (1971) Correlation of pemphigoid and pemphigus antibody titres with activity of disease. *Br J Dermatol* 84:7–13

Sekiguchi M, Futei Y, Fujii Y, Iwasaki T, Nishikawa T, Amagai M (2001) Dominant autoimmune epitopes recognized by pemphigus antibodies map to the N-terminal adhesive region of desmogleins. *J Immunol* 167:5439–48

Shirakata Y, Amagai M, Hanakawa Y, Nishikawa T, Hashimoto K (1998) Lack of mucosal involvement in pemphigus foliaceus may be due to low expression of desmoglein 1. *J Invest Dermatol* 110:76–8

Tsunoda K, Ota T, Aoki M, Yamada T, Nagai T, Nakagawa T *et al.* (2003) Induction of pemphigus phenotype by a mouse monoclonal antibody against the amino-terminal adhesive interface of desmoglein 3. *J Immunol* 170:2170–8

Tsunoda K, Ota T, Suzuki H, Ohyama M, Nagai T, Nishikawa T *et al.* (2002) Pathogenic autoantibody production requires loss of tolerance against desmoglein 3 in both T and B cells in experimental pemphigus vulgaris. *Eur J Immunol* 32:627–33

Original Article

Cytogenet Genome Res 115:51–61 (2006)
DOI: 10.1159/000094801

Cytogenetic and Genome Research

Genomic structure of swine taste receptor family 1 member 3, *TAS1R3*, and its expression in tissues

S. Kiuchi[a] T. Yamada[b] N. Kiyokawa[c] T. Saito[a] J. Fujimoto[c] H. Yasue[a]

[a]National Institute of Agrobiological Sciences, Tsukuba, Ibaraki
[b]School of Medicine, Keio University, Shinjuku-ku
[c]National Research Institute for Child Health and Development, Setagaya-ku, Tokyo (Japan)

Manuscript received 18 October 2005; accepted in revised form for publication by H. Hameister, 9 February 2006.

Abstract. Taste receptor family 1 member 3, TAS1R3, is shown to be involved in sweet and umami tastes in mouse, and the nucleotide sequence of the gene has been reported in rat, gorilla, and human. Pigs are frequently used as models for human diseases, and are also considered to be source animals for xenotransplantation to humans due to their anatomical and physiological similarities to humans. Therefore, in the present study, the genomic structure of the swine *TAS1R3* gene was determined, and *TAS1R3* expression was studied in various swine tissues. The gene was shown to reside on swine chromosome 6q22→q23, from which three types of mRNAs were generated: 3,752 bp derived from six exons in tongue, 3,704 bp from six exons and 3,630 bp from seven exons in testis. The 6 exons/5 introns were structurally similar to those of humans and mice, but the 7 exons/6 introns structure of *TAS1R3* was first observed in swine. High expressions of *TAS1R3* were revealed in tongue, kidney, and testis by real-time PCR. The expression profile of the tissues except for kidney was similar to that of mouse. When in situ hybridization using an RNA probe for *TAS1R3* was performed on swine tongue and testis tissues, *TAS1R3* expressions were revealed in tongue circumvallate papillae, fungiform papillae, mucosal epithelium, follicular B lymphocytes, lymphocytes in submucosal tissues of lingual tonsil, and spermatogenic cells. Using peripheral mature B lymphocytes, the expression of *TAS1R3* in B lymphocytes was further confirmed by real-time PCR and sequencing of the real-time PCR product.

Taste consists of five modalities, that is, salty, sour, bitter, sweet, and umami. These modalities are necessary for growth and survival in animals. Physiological studies have indicated that taste receptor cells selectively respond to different tastants (Gilbertson et al., 1992; Bernhardt et al., 1996; Cummings et al., 1996). Electro-physiological studies have suggested that salty and sour tastants modulate taste receptor cell function by directly affecting specialized membrane channels (Kretz et al., 1999; Lin et al., 2004). On the other hand, taste responses to bitter, sweet, and umami are shown to be initiated by G-protein-coupled receptors (GPCRs) and transduced via G-protein signaling cascades (Gilbertson et al., 2000; Lindemann, 2001). Bitter tastants are detected by ~30 members of the taste receptor family 2 (TAS2R), a subfamily of the GPCRs. Most TAS2Rs are co-expressed in the same subset of taste receptor cells (Adler et al., 2000), suggesting that these cells function as generalized bitter detectors. Sweet and umami tastes are mediated by three members of the taste receptor family 1 (TAS1R), a distinct GPCR subfamily. TAS1Rs combine to assemble two heteromeric GPCR complexes. The complex of taste receptor family 1 member 2 (TAS1R2) and taste receptor family 1 member 3 (TAS1R3) serves as a sweet taste receptor (Nelson et al., 2001; Li et al., 2002; Zhao et al., 2003); and that of

Request reprints from Hiroshi Yasue
Genome Research Department
National Institute of Agrobiological Sciences, 2 Ikenodai
Tsukuba, Ibaraki 305-0901 (Japan)
telephone: +81-298-38-8664; fax: +81-298-38-8674
e-mail: hyasue@affrc.go.jp

1424–8581/06/1151–0051$23.50/0

Accessible online at:
www.karger.com/cgr

taste receptor family 1 member 1 (TAS1R1) and TAS1R3, as an umami taste receptor (Li et al., 2002; Nelson et al., 2002; Zhao et al., 2003). In the genetic analysis of mice strains showing differences in preference for sweet, it is suggested that the sequence polymorphisms causing amino-acid substitutions are associated with this preference (Max et al., 2001; Reed et al., 2004).

Recently, pigs have drawn the attention of many researchers not only as a model animal for human diseases but also as a resource for xenotransplantation to humans because of their anatomical and physiological similarities to humans (Tumbelson and Schook, 1996). In line with this and the fact that elucidation of the preferences in pig populations would help breeding in terms of feeding efficiency (one of the major factors in animal science), in the present study we have determined the genomic structure of swine *TAS1R3* and investigated the mode of *TAS1R3* gene expression in various tissues. The swine *TAS1R3* gene is similar to that of human and mouse with respect to its reported genome structure and expression. Furthermore, the present study for the first time has revealed an alternative splicing of *TAS1R3* in testis and *TAS1R3* expression in tongue mucosal epithelium, mature B lymphocytes, and spermatogenic cells. This may imply as yet unreported additional functions of TAS1R3.

Materials and methods

Pigs for preparation of tissues and cells

Three and a half month-old male pigs of Landrace or Landrace/Duroc/Largewhite composite were used to obtain tissue for both RNA and in situ gene expression analyses. The animals used in the present study received humane care as described in the Guidelines for the Care and Use of Experimental Animals (National Institute of Agrobiological Sciences Care Committee, Japan). Peripheral blood cells obtained from these pigs were applied to a cell-sorter (EPICS ALTRA; Beckman Coulter, CA, USA) using anti-CD21 antibody (VMRD, Inc., WA, USA) to obtain a mature B lymphocyte population. The process for the preparation of tissue samples followed the guidelines of animal ethics at the National Institute of Agrobiological Sciences. The pigs were euthanized by an intravenous injection of 10 ml of sodium pentobarbital. Immediately after respiration and heartbeat stopped, tissue samples were excised from tongue, heart, lung, stomach, intestine, liver, kidney, and testis to prepare RNA and to fix tissues in 4% (w/v) paraformaldehyde in phosphate-buffered saline.

Analysis of swine TAS1R3 gene structure

To obtain bacterial artificial chromosome (BAC) clones containing the *TAS1R3* gene, a swine genomic DNA BAC library constructed by Suzuki et al. (2000) was screened by PCR. Primers (forward: hT1R3-Ex2L, reverse: hT1R3-Ex2R in Table 1) for PCR were designed from the human sequence (GenBank/EMBL/DDBJ Data Bank Accession No. BK000152) showing a high similarity to the mouse *Tas1r3* sequence (Accession No. AF337039, AL670236.9). The fragment (200 bp) amplified from swine genomic DNA by PCR using the primers was sequenced to confirm that the sequence was orthologous to that of human *TAS1R3*. BAC clones were subsequently selected from the library, and the purified BAC-DNA was cleaved with *Hin*dIII, fractionated by electrophoresis, and hybridized with a digoxigenin-labeled swine DNA fragment amplified by the above primers (PCR DIG Probe Synthesis Kit: Roche Diagnostics, Mannheim, Germany). BAC-DNA fragments which hybridized to the digoxigenin-labeled fragment were subcloned into pBluescript KS(+) and sequenced using PRISM Ready Reaction BigDye Terminator Cycle Sequencing Kits (ver. 2) (Applied Biosystems, Calif., USA) and an ABI3100 DNA sequencer (Applied Biosystems).

Preparation of porcine RNA

RNA was prepared from 0.7–1.7 g tissue samples using the guanidinium thiocyanate acid-phenol-chloroform method with TRIzol reagent (Invitrogen, Calif., USA) and from the mature B lymphocytes using RNeasy (QIAGEN Sciences, Md., USA). The RNAs thus prepared were treated with DNase I (TAKARA, Shiga, Japan) at 37°C for 30 min, and then with phenol:chloroform. The amounts and purities of the resulting RNAs were estimated by their absorbance from 220 to 320 nm.

Analysis of TAS1R3 cDNA

First-strand cDNA was prepared from the RNA obtained by the above, following the procedure described by Suzuki and Sugano (2003), and then used to amplify the *TAS1R3*-specific DNA fragments by PCR using primer pairs (see Table 1) designed with a swine *TAS1R3* genomic sequence. Briefly, PCR was performed in a 50 μl reaction mixture containing 2 μl of the tongue or testis first-strand cDNA as a template, LA PCR buffer (without $MgCl_2$) (TAKARA), 1.5 mM $MgCl_2$, 400 μM dNTPs, 0.05 U/μl TaKaRa LA Taq (TAKARA) and 0.2 μM primer pair (forward: T1R3-ExStaF, reverse: T1R3-3R), as indicated in Table 1. PCR was carried out at 94°C for 1 min, followed by 40 cycles of PCR consisting of 30 s denaturation at 94°C, 30 s annealing at 60°C, and 4 min extension at 72°C, and finally an extension step at 72°C for 10 min. Secondary PCR was performed using an aliquot of the preceding PCR product and a nested pair of primers (forward: T1R3-ExStaF, reverse: T1R3-ExEndR) (Table 1). Amplified PCR fragments were cloned into pUC118 and sequenced by the primer-walking method.

In order to obtain the 5′ and 3′ terminal regions of the *TAS1R3* transcripts, 5′ and 3′ rapid-amplification-of-cDNA ends (RACE) analysis was performed with the 5′/3′ RACE kit (Roche Diagnostics), following the manufacturer's instructions. The primer pairs for the RACE analysis are described in Table 1. The DNA fragments obtained by the RACE analysis were cloned and sequenced as above.

Attempts to identify SNPs (single nucleotide polymorphisms) of TAS1R3 possibly related to tasting

The genomic DNAs of a swine from each of five breeds, viz, Göttingen, Largewhite, Duroc, Berkshire, and Japanese wild boar, two from Landrace, and two F_1 from a Meishan × Göttingen cross population (Mikawa et al., 1999) were sequenced to identify sequence polymorphisms for the sweet preference, as in mouse (Max et al., 2001; Reed et al., 2004).

Assignment of TAS1R3 to the IMpRH map

In order to assign *TAS1R3* to the IMpRH map (http://imprh.toulouse.inra.fr/), primer pairs were designed in the sequence of *TAS1R3* and examined to select those which amplified the expected sequences from swine genomic DNA but not from Chinese hamster genomic DNA. One of the primer pairs (forward: H6-2-R2, reverse: T1R3-Ex1R in Table 1) was used for typing of IMpRH panel DNAs which had been kindly provided by INRA (France) and the University of Minnesota (USA) for radiation hybrid (RH) mapping (Yerle et al., 1998). The typing procedure was the same as that described previously (Kiuchi et al., 2002). The typed data were submitted to the IMpRH server at http://imprh.toulouse.inra.fr/ (Milan et al., 2000) to obtain the likely position of *TAS1R3* on the IMpRH map.

Fluorescence in situ hybridization localization of TAS1R3 on swine chromosome

Swine peripheral blood cells (Landrace) were cultured and labeled with 5-BrdU as described previously (Awata et al., 1995). The cultured cells were treated with hypotonic solution and fixative, followed by spreading on glass slides as described previously (Yasue and Ishibashi, 1982). Chromosome spreads were then subjected to FISH as described previously (Awata et al., 1995) using probe DNA. For the probe DNA, BAC DNA (500 ng) containing the *TAS1R3* gene was labeled with biotin using a nick translation kit (Roche Diagnostics).

Table 1. Primer list

Project / Primer name	Primer positions[a] from / to	Sequence (5′–3′)	Size (mer)	Annealing temperature (°C)	PCR product size (bp)
BAC library screening /					
hT1R3-Ex2L (forward)		CTACGACCTCTTTGATACGTGCTC	24	61	200
hT1R3-Ex2R (reverse)		GCATGAGGAAGAAGCTGAAGAACT	24		
1st-PCR for cDNA cloning /					
T1R3-ExStaF (forward)	−37 / −16	TGCTCACTGCCATCCCTGCTGG	22	60	3,321
T1R3-3R (reverse)	+3828 / +3807	ACCCATGACTGGCTTGGTACTG	22		
2nd-PCR for cDNA cloning /					
T1R3-ExStaF (forward)	−37 / −16	TGCTCACTGCCATCCCTGCTGG	22	60	2,627
T1R3-ExEndR (reverse)	+3134 / +3113	GGCACCTTGACTACGTCTGAGG	22		
Synthesis of 1st-strand cDNA in 5′RACE /					
T1R3-Ex3R	+701 / +682	GAAGAAGGAGGGGAACGTCT	20		
1st-PCR in 5′RACE /					
Oligo dT-anchor primer (forward) (Roche)		GACCACGCGTATCGATGTCGACTTTTTTTTTTTTTTTV	39	57	
T1R3-Ex2R3 (reverse)	+541 / +522	AGCCGAAGAACTTGCCGGTG	20		
2nd-PCR in 5′RACE /					
PCR anchor primer (forward) (Roche)		GACCACGCGTATCGATGTCGAC	22	59	
T1R3-Ex1R (reverse)	+104 / +84	AGCACGTAGTGCCCTTGCATG	21		
1st-PCR in 3′RACE /					
T1R3-Ex67F (forward)	+2839 / +2859	CATGCTGGCCTACTTCATCAC	21	57	
PCR anchor primer (reverse) (Roche)		GACCACGCGTATCGATGTCGAC	22		
2nd-PCR in 3′RACE /					
T1R3-Ex67F2 (forward)	+2967 / +2986	ACCTGCCCAAGTGCTACCTG	20	59	
PCR anchor primer (reverse) (Roche)		GACCACGCGTATCGATGTCGAC	22		
RH mapping /					
H6-2-R2 (forward)	−203 / −182	GGTGGCATCAGAATAAGAGTCC	22	59	307
T1R3-Ex1R (reverse)	+104 / +84	AGCACGTAGTGCCCTTGCATG	21		
Real-time PCR for *TAS1R3* /					
tg-502T (TaqMan probe)		CCACCGTGTGTACCAGGTTCTCGTC	25		
tg-476F (forward)	+144 / +160	GCTGGGCGACAGGACAG	17	50	102
tg-577R (reverse)	+317 / +298	TTGATTTCCTCCACAGCCAT	20		
RNA synthesis from *EGFP* /					
T7p-EGFP-540F (forward)		AGTAATACGACTCACTATAGGGCGACCACTACCAGCAGAACA	42	59	218
dT18-EGFP-717R (reverse)		TTTTTTTTTTTTTTTTTTCTTGTACAGCTCGTCCATGC	38		
Real-time PCR for *EGFP* /					
FAM-EGFP-634T (TaqMan probe)		CCCAACGAGAAGCGCGATCACA	22		
U57608EGFP615F (forward)		GTCCGCCCTGAGCAAAGA	18	50	62
U57608EGFP676R (reverse)		TCACGAACTCCAGCAGGACC	20		
Synthesis of ISH Anti-Sense cRNA probe /					
T1R3-71F (forward)	+2854 / +2873	CATCACCTGGGTTTCCTTTG	20	57	165
T7-prm-T1R3-72R (reverse)	+2996 / +2977	AGTAATACGACTCACTATAGGGACCTCAGCAGCAGGTAGCAC	42		
Synthesis of ISH Sense cRNA probe /					
T7-prm-T1R3-71F (forward)	+2854 / +2873	AGTAATACGACTCACTATAGGGCATCACCTGGGTTTCCTTTG	42	57	165
T1R3-72R (reverse)	+2996 / +2977	ACCTCAGCAGCAGGTAGCAC	20		

[a] Positions based on the nucleotide number shown in Fig. 1.

Measurement of TAS1R3 gene expression by real-time PCR

An aliquot of each RNA sample was mixed with an amount of RNA fragment synthesized from pEGFP-C1 vector (EGFP: enhanced green fluorescent protein, Invitrogen), and the resulting mixture was subjected to synthesis of the first-strand cDNA using SuperScript III (Invitrogen), 5 μM Random Hexamer and 500 μM dNTPs, following the manufacturer's procedure. The RNA fragment from EGFP was prepared using a primer pair (forward: T7p-EGFP-540F, reverse: dT18-EGFP-717R in Table 1) with the AmpliScribe T7 High Yield Transcription Kit (EPICENTRE, Wisc., USA), and was then used as a monitor for reverse transcription efficiency and a standard for a quantitative comparison of *TAS1R3* transcripts among the samples. Samples subjected to synthesis of the first-strand cDNA were treated with RNaseH (TOYOBO, Osaka, Japan) at 37°C for 20 min. First-strand cDNA derived from *TAS1R3* transcripts in the samples was detected using TaqMan Universal Master Mix (Applied Biosystems), TaqMan probe (tg-502T) and the primer pair (forward: tg-467F, reverse: tg-557R), according to the procedure recommended by Applied Biosystems (ABI 7700). The first-strand cDNA derived from EGFP RNA was detected using TaqMan Universal Master Mix (Applied Biosystems), TaqMan probe (FAM-EGFP-634T) and a primer pair (forward: U57608EGFP615F, reverse: U57608EGFP676R). Primer sequences are listed in Table 1.

Prior to measurement, the fragment amplified from the tongue sample with the primer pair for *TAS1R3* was sequenced to confirm that

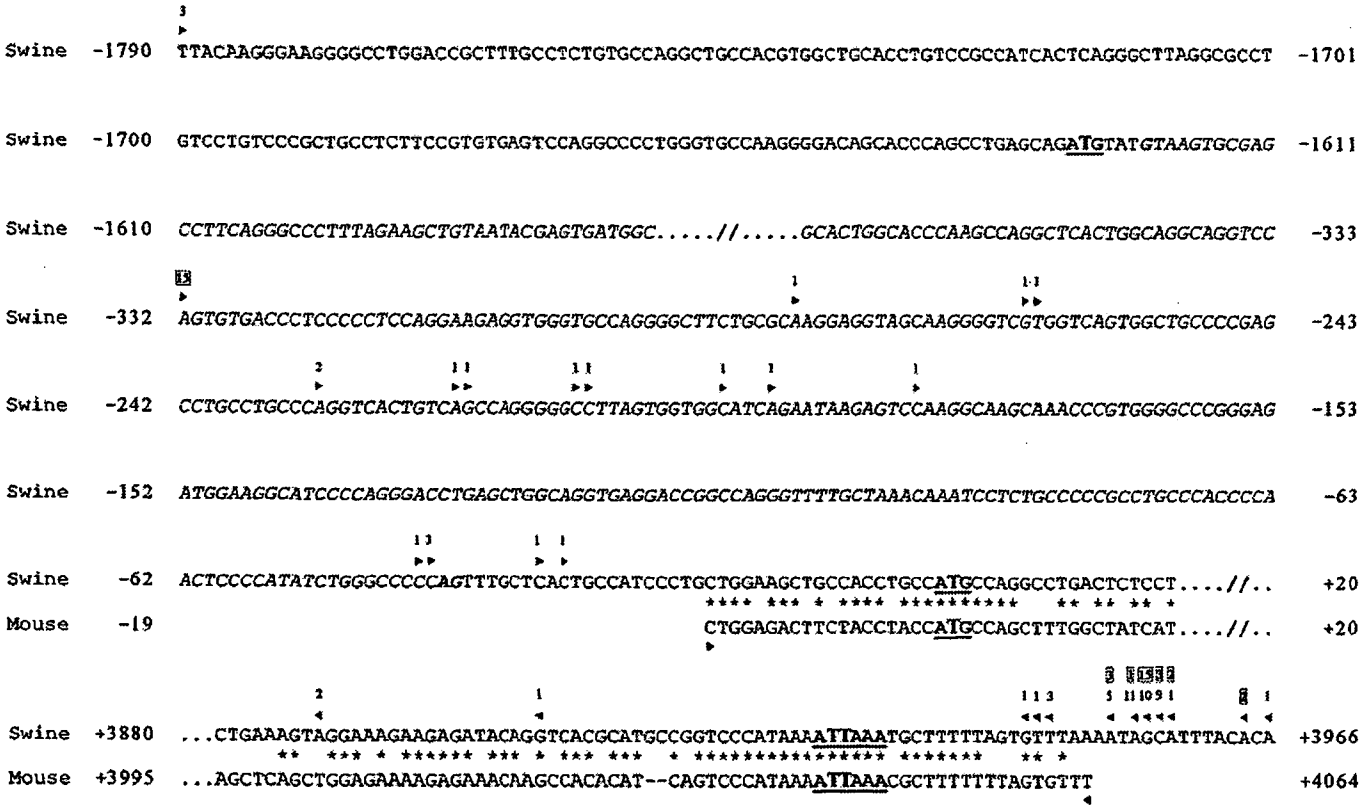

Fig. 1. Transcription initiation and termination sites of swine *TAS1R3*. The *TAS1R3* genomic sequence was numbered downstream of the transcription with the putative translation start site of Tongue1 as +1. That start site and polyadenylation signal site are denoted by bold letters and underlines. The sequence indicated to be the intron for Tes2 transcription is shown in italics. Downstream arrowheads with boxed and unboxed numerals indicate initiation sites of the transcription in tongue and testis, respectively. Upstream arrowheads with boxed and unboxed numerals indicate termination sites of the transcription in tongue and testis, respectively. The numerals represent the number of clones showing initiation or termination of the transcription at the site of each arrowhead in the RACE analysis. As a reference, part of the mouse sequence was aligned with a swine sequence to show the transcription initiation and termination sites reported in mouse (Accession No. AF337039 and AL670236.9).

the primer pair amplified the expected sequence. In addition, it was confirmed that the DNA fragment from EGFP RNA was proportionally amplified depending on the amount of EGFP RNA used for real-time PCR.

Detection of gene expression site in tissues by in situ hybridization

After dissected tissues were fixed overnight in paraformaldehyde solution, they were embedded in paraffin and then sectioned 4 μm thick. Sections were collected on glass-slides and subjected to in situ hybridization. The procedure for in situ hybridization was the same as that reported earlier (Ohtsuki et al., 1998) with the following exception: hybridization was performed in a solution containing 50% formamide, 2× SSC, 1.0 mg/ml tRNA, 1.0 mg/ml salmon sperm DNA, 1.0 mg/ml BSA, 10% dextran sulfate, 1.0% SDS, and 8.0 μg/ml RNA anti-sense or sense probe at 37°C for 16 h. Hybridization signals were detected with the NBT/BCIP system (Sigma-Aldrich, Mo., USA).

For the RNA probe, DNA fragments were first prepared by PCR from *TAS1R3* cDNA using primer pairs T1R3-71F:T7-prm-T1R3-72R, and T7-prm-T1R3-71F:T1R3-72R. The sequences of primers are listed in Table 1. Using the DNA fragment obtained with the primer pair T1R3-71F:T7-prm-T1R3-72R and using the AmpliScribe T7-Flash Transcription Kit (EPICENTRE), a digoxigenin-labeled RNA anti-sense probe was prepared according to the manufacturer's instructions. With the same procedure, a digoxigenin-labeled RNA sense probe was prepared using the DNA fragment obtained with the primer pair T7-prm-T1R3-71F:T1R3-72R.

Results

TAS1R3 gene

A swine genomic DNA BAC library was screened to obtain three BAC clones containing at least a part of the putative *TAS1R3* gene. DNA from the BAC clones was processed as described in Material and methods to identify a *Hin*dIII fragment (about 6.6 kb) that contained the putative *TAS1R3* gene. The 6.6 kb fragment of one BAC clone (code 994D12) was cloned in pBluescript KS(+) and sequenced. In addition, cDNA fragments (2,627 bp) of *TAS1R3* transcripts from tongue tissue were generated using the primer pairs listed in Table 1, cloned into pUC118 vector, and sequenced. Since 5′/3′ regions of the putative *TAS1R3* gene transcript were likely to be missing from the cDNA sequences, RACE analysis was performed using the RNA prepared from tongue to determine the sequences of the 5′/3′ terminal regions. Fifteen fragments obtained by 5′ RACE were sequenced, revealing that all the transcriptions initiated from nucleotide position −332 (numbered from the translation start nucleotide in the 3′-direction in the present study). The sequenc-

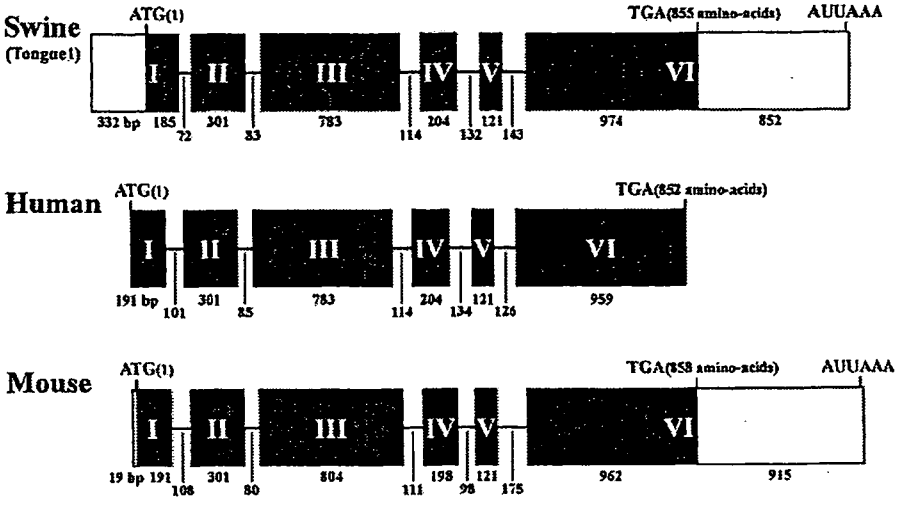

Fig. 2. Schematic presentation of swine *TAS1R3* gene structure. Boxes denote exons, with white parts representing 5'-untranslated region (UTR) and 3'UTR; and black parts signifying protein-coding regions. Exons are numbered according to their correspondence with those of human and mouse. As a reference, the genomic structures of human and mouse *TAS1R3* genes are included in this figure. The accession numbers for human and mouse cDNA of *TAS1R3* genes are BK000152 and AF337039, respectively. Those for human and mouse genomic DNA are NT_077965.1 and AL670236.9, respectively.

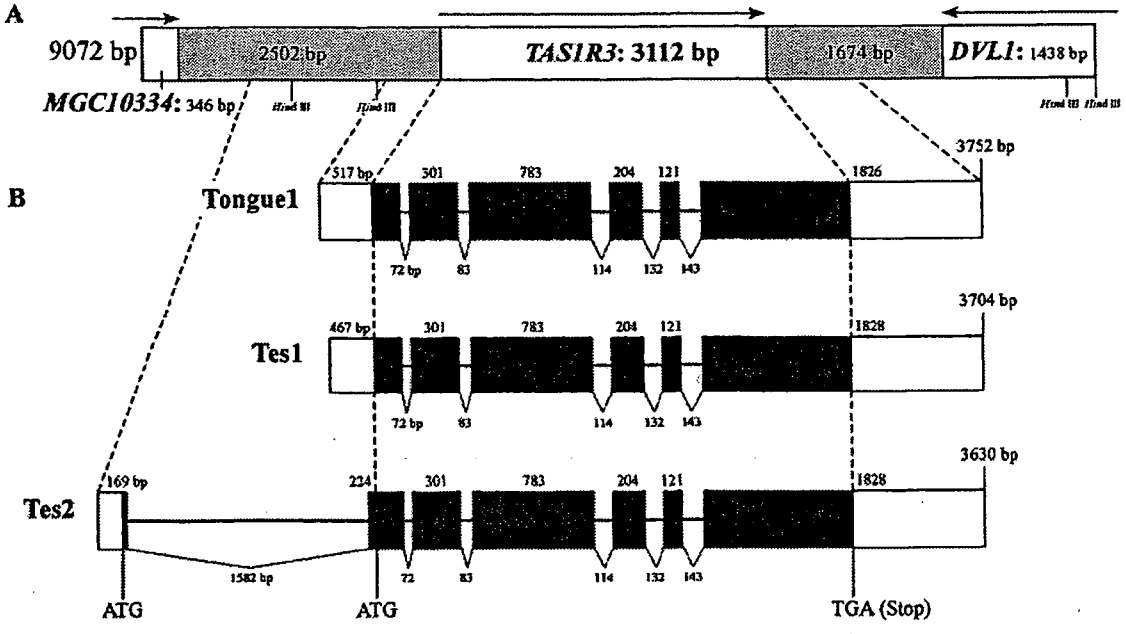

Fig. 3. Correspondence of swine *TAS1R3* transcripts to genomic sequence. (**A**) Swine genomic structure of the region encompassing *TAS1R3*. Regions tagged with *MGC10334* and *DVL1* correspond to human *MGC10334* and *DVL1*, respectively, based on sequence similarities. (**B**) Swine *TAS1R3* genomic structures, from which *TAS1R3* transcripts, Tongue1, Tes1, and Tes2, were derived. The reconstituted longest transcript in each type is presented in this figure. Symbols and markings in this figure are the same as those in Fig. 2.

ing of 26 fragments in 3' RACE demonstrated that the transcriptions terminated at the nucleotide positions ranging from +3953 to +3964 (Fig. 1).

The reconstituted longest cDNA sequence (3,752 bp; from −332 to +3964 of the swine genomic sequence) (Tongue1: Accession No. AB162127) was then compared with the swine genomic sequence determined in the present study, revealing that swine putative *TAS1R3* consists of six exons and five introns, spanning 4,296 bp (Accession No. AB162126) (Fig. 2). When the structure of the putative *TAS1R3* gene was compared with those of human and mouse *TAS1R3* genes, it was found that their genomic structures were the same, though slight differences in the lengths of exons and introns were observed (Fig. 2). When the protein-coding sequence of Tongue1 was compared with that of human and mouse, the similarities between swine and human, and between swine and mouse were found to be 81.1% and 73.9%, respectively. These findings taken together led us to

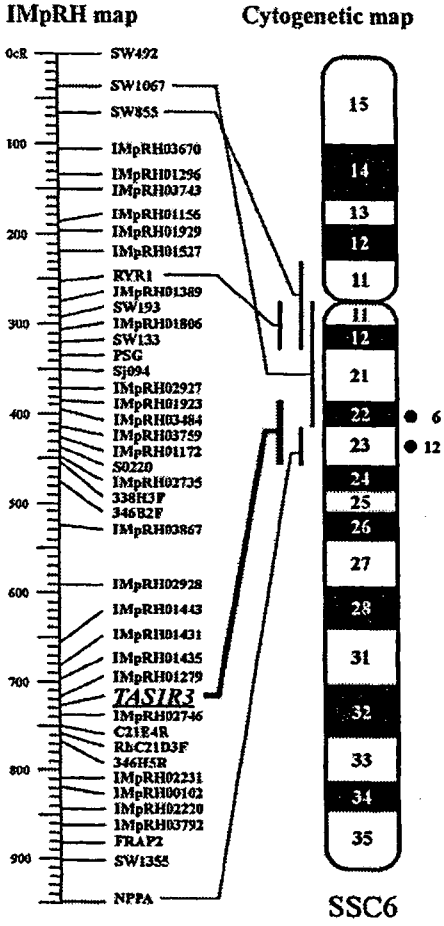

Fig. 4. Chromosomal location of swine *TAS1R3*. The position of *TAS1R3* (shown with italic and underline) on the IMpRH map was indicated. *TAS1R3* was assigned to the map by the RH mapping procedure described in Materials and methods (http://imprh.toulouse.inra.fr/). In addition, the chromosomal position of *TAS1R3* was determined by FISH, also described in Materials and methods. Hybridization signals obtained in FISH were scored along bands of the SSC6 ideogram, and presented as closed circles with the number of signals scored.

conclude that this swine putative *TAS1R3* gene is the orthologue of human and mouse *TAS1R3* genes.

Max et al. (2001) observed that *TAS1R3* mRNA of mouse testis showed a size difference from that of mouse tongue. Therefore, swine *TAS1R3* mRNA derived from testis was examined as in the case of tongue mRNA. This analysis revealed that two types of mRNA were generated from the *TAS1R3* gene in testis: one (Tes1: Accession No. AB162128) was the same as the tongue type, except that its transcription initiation sites varied in range from -282 to -31; the other (Tes2: Accession No. AB162129) contained an additional 45-bp protein-coding sequence upstream from the translation start site observed in Tongue1 and Tes1, which provided an additional 15 amino-acids to the deduced TAS1R3 protein encoded by Tongue1 and Tes1. The transcription termination sites of Tes2 were found to be similar to those of Tongue1 and Tes1. In order to determine the genomic structure for Tes2 production, the BAC-DNA was additionally sequenced, and compared with Tes2 sequences. It was revealed that Tes2 was derived from seven exons, which is the result of alternative splicing of *TAS1R3* as shown in Fig. 3.

Chromosomal assignment of TAS1R3

The swine genomic sequence containing *TAS1R3* (Accession No. AB162126) was compared with the corresponding human and mouse sequences. That comparison demonstrated that the arrangement of genes, i.e., *MGC10334-TAS1R3-DVL1* in swine (Fig. 3A), was the same as that of human and mouse, showing that the genomic region encompassing *TAS1R3* has been conserved at least in those three species. RH mapping was performed to assign the gene to the IMpRH map of swine chromosome (SSC) 6 between IMpRH01279 and IMpRH02746 (Fig. 4). We also carried out FISH to locate the gene physically on SSC6. FISH, as shown in Fig. 4, demonstrated that *TAS1R3* resides on SSC6q22→q23; this result is consistent with that of RH mapping.

Amino-acid sequence of TAS1R3

The amino-acid sequences derived from Tongue1 (or Tes1) and Tes2 were aligned with human and mouse TAS1R3 (Fig. 5). Based on the annotation of human and mouse TAS1R3, a signal peptide (http://www.cbs.dtu.dk/services/SignalP/), an ANF-receptor domain (receptor family ligand binding region), and a 7tm_3 domain (metabotropic glutamate family) (http://www.ncbi.nlm.nih.gov/BLAST/) were identified in the swine TAS1R3 amino-acid sequence of the alignment (Fig. 5).

When swine TAS1R3 derived from Tongue1 (or Tes1) was compared with that of human and mouse, the overall similarities of TAS1R3s between swine and human and between swine and mouse were calculated to be 75.1% and 71.6%, respectively. The similarities between swine and human, and between swine and mouse for the signal peptide region were calculated to be 47.1% and 50.0%, respectively, while those for the ANF-receptor domain were 74.5% and 72.6%, and those for the 7tm_3 domain were 81.7% and 76.6%, respectively. The borders between exons for swine, human, and mouse all occurred at the same positions in the alignment shown in Fig. 5, which is additional evidence for the similarity of the *TAS1R3* gene among the three species.

Since an additional 15 amino-acids were observed at the N-terminus of the protein derived from Tes2 compared to that from Tongue1 (or Tes1), the deduced amino-acid sequence from Tes2 was subjected to a web analysis for signal

Fig. 5. Alignment of swine, human and mouse TAS1R3 amino-acid sequences. The protein deduced from Tongue1/Tes1 comprises 855 amino-acids, and that from Tes2 870 amino-acids. Amino-acid sequences of proteins were aligned with human and mouse TAS1R3 using Genetyx (Software Development Co., Ltd., Tokyo, Japan). The amino-acids of Tes2 identical to those of Tongue1/Tes1 are shown by dots.

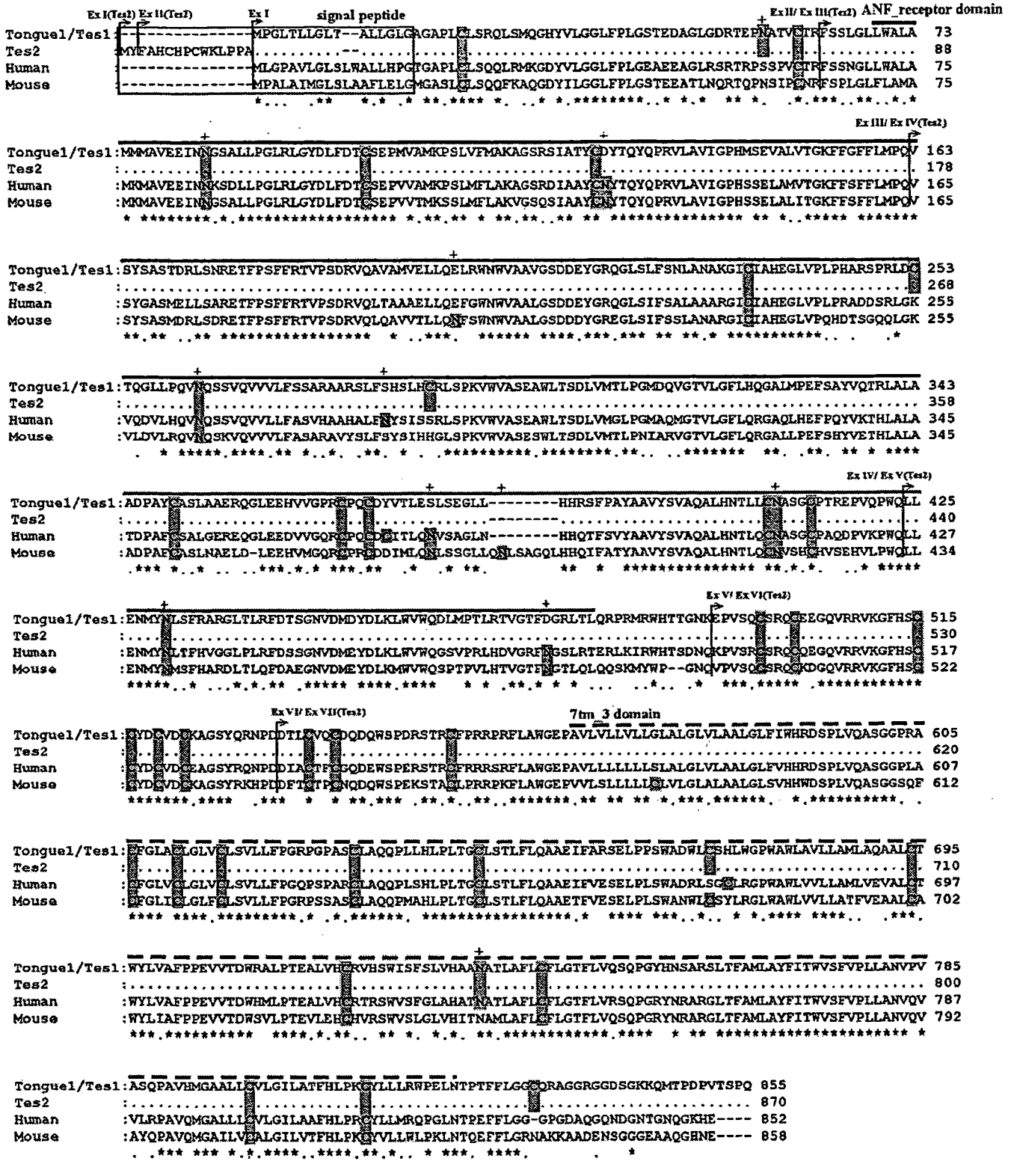

Putative signal peptide (http://www.cbs.dtu.dk/services/SignalP/) is boxed. The putative ANF-receptor domain (http://www.ncbi.nlm.nih.gov/Structure/cdd/cddsrv.cgi?uid=pfam01094&version=v2.04) and putative seven transmembrane domain (7tm_3 domain; http://www.ncbi.nlm.nih.gov/Structure/cdd/cddsrv.cgi?uid=pfam00003&version=v2.04) are marked by the solid and broken lines over the sequence, respectively. Potent N-linked glycosylation sites and cysteine residues are indicated by gray boxes with and without '+', respectively. Amino-acids conserved among swine, human, and mouse in the alignment are indicated by asterisks. Four out of six potent N-linked glycosylation sites and 29 out of 33 cysteine residues in swine are conserved in the three species.